Bornavirus closely associates and segregates with host chromosomes to ensure persistent intranuclear infection.

AUTHOR(S):

Matsumoto, Yusuke; Hayashi, Yohei; Omori, Hiroko; Honda, Tomoyuki; Daito, Takuji; Horie, Masayuki; Ikuta, Kazuyoshi; ... Yoshimori, Tamotsu; Schwemmle, Martin; Tomonaga, Keizo

CITATION:

Matsumoto, Yusuke ...[et al]. Bornavirus closely associates and segregates with host chromosomes to ensure persistent intranuclear infection.. Cell host & microbe 2012, 11(5): 492-503

ISSUE DATE:

2012-05-17

URL:

http://hdl.handle.net/2433/156163

Cell Host & Microbe

Bornavirus closely associates and segregates with host chromosomes to ensure persistent intranuclear infection

Yusuke Matsumoto[a,b,1], Yohei Hayashi[b,1,2], Hiroko Omori[c], Tomoyuki Honda[a], Takuji Daito[a,3], Masayuki Horie[a,d], Kazuyoshi Ikuta[b], Kan Fujino[a,b], Shoko Nakamura[a], Urs Schneider[d], Geoffrey Chase[d], Tamotsu Yoshimori[e], Martin Schwemmle[d] and Keizo Tomonaga[a,f,4]

[a]*Department of Viral Oncology, Institute for Virus Research, Kyoto University, Kyoto 606-8507, Japan,* [b]*Department of Virology and* [c]*Central Instrumentation Laboratory, Research Institute for Microbial Diseases (BIKEN), Osaka University, Osaka 565-0871 Japan,* [d]*Department of Virology, Institute for Medical Microbiology and Hygiene, University of Freiburg, D-79104 Freiburg, Germany,* [e]*Department of Genetics, Osaka University Graduate School of Medicine, 2-2 Yamadaoka, Suita, Osaka 565-0871 Japan, and* [f]*PRESTO, Japan Science and Technology Agency (JST), Chiyoda-ku, Tokyo 102-0075, Japan.*

[1]These authors contributed equally to this work. [2]Present address; Microbiological Research Institute, Otsuka Pharmaceutical Co., Ltd. 463-10 Kagasuno, Kawauchi-cho, Tokushima 771-0192, Japan. [3]Present address; National Institute of Infectious Diseases, Department of Virology II, 1-23-1 Toyama, Shinjuku-ku, Tokyo 162-8640, Japan.

[4]To whom correspondence should be addressed. Dr. Keizo Tomonaga: Department of Viral Oncology, Institute for Virus Research, Kyoto University, 53 Kawahara-cho, Shogoin, Sakyo-ku, Kyoto 606-8507, Japan. Tel: +81-75-751-3997, Fax: +81-75-751-4000, E-mail: tomonaga@virus.kyoto-u.ac.jp

SUMMARY

Bornaviruses are nonsegmented negative-strand RNA viruses that establish a persistent infection in the nucleus and integrate occasionally a DNA genome copy into the host chromosomal DNA. However, how these viruses achieve intranuclear infection remains unclear. We show that Borna disease virus (BDV), a mammalian bornavirus, closely associates with the cellular chromosome to ensure intranuclear infection. BDV generates viral factories within the nucleus using host chromatin as a scaffold. In addition, the viral ribonucleoprotein (RNP) interacts directly with the host chromosome throughout the cell cycle, using core histones as a docking platform. HMGB1, a host chromatin-remodeling DNA architectural protein, is required to stabilize RNP on chromosomes and for efficient BDV RNA transcription in the nucleus. During metaphase, the association of RNP with mitotic chromosomes allows the viral RNA to segregate into daughter cells and ensure persistent infection. Thus, bornaviruses likely evolved a chromosome-dependent lifecycle to achieve stable intranuclear infection.

INTRODUCTION

The cell nucleus is a dynamic organelle that may be considered an inconvenient site for virus infection. Dissolution of the nuclear membrane during mitosis and nucleocytoplasmic trafficking through nuclear pores could lead to the loss or dilution of viral genomes from the nucleus. Alteration of the intranuclear environment by gene expression may also affect virus stability. For persistent DNA viruses, such as gammaherpesviruses and papillomaviruses, association of a low copy number of viral episomal DNA with cellular chromosomes ensures their stable retention over long periods of time in such a dynamic environment (Ballestas et al., 1999; Feeney and Parish, 2009; Lehman and Botchan, 1998; Piolot et al., 2001). Residence in the nucleus, however, would not be an easy task for other types of viruses, in particular viruses using RNA as the template for replication.

Among vertebrate RNA viruses, except for the reverse-transcribing retroviruses, only two families, *Bornaviridae* and *Orthomyxoviridae*, enter the nucleus for replication and transcription. However, there is a fundamental difference between these two viruses. Bornaviruses replicate non-cytopathically and readily establish a long-lasting, persistent infection in the nuclei of cultured cells and various tissues (Schneider et al., 2007; Tomonaga et al., 2002), whereas a consequence of infection by influenza virus, belonging to the *Orthomyxoviridae*, is induction of apoptotic cell death. Thus, bornaviruses are the only known RNA viruses that can parasitize within the nuclear membrane.

Borna disease virus (BDV) is the prototype bornavirus and is known to infect many mammalian species (Schneider, 2005; Staeheli et al., 2000). A unique feature of BDV is that only a small number of infectious particles are released from infected cells (Gonzalez-Dunia

et al., 1997; Tomonaga et al., 2002). Nevertheless, the copy number of the viral genomic RNA (vRNA) is maintained during the persistence of BDV in the nucleus. Recently, we have reported that BDV generates DNA forms of its own mRNA in infected cells, and integrates DNA copies of the nucleoprotein (N) mRNA into the host genome (Horie et al., 2010). Furthermore, we found that bornaviruses have left their own endogenous elements in the genomes of several animal species, including humans, non-human primates and rodents, as a "fossil record" of ancient bornavirus infection (Belyi et al., 2010; Horie et al., 2010). However, the fundamental question of how bornaviruses can achieve such a stable intranuclear infection has not been elucidated.

In this study, we analyzed in detail the intranuclear dynamics of BDV to understand the unique life cycle of bornavirus in the nucleus. We showed that BDV generates spheroidal viral factories in the nucleus, using chromatin environments as a scaffold for the structure. In addition, the BDV ribonucleoprotein (RNP) was seen to be tightly associated with condensed chromosomes upon mitosis and to segregate into daughter cell nuclei along with mitotic chromosomes. Immunoprecipitation analysis of the chromatin-binding fraction revealed that core histones are the docking partners of viral RNP to chromatin. Furthermore, we showed that the chromatin-remodeling, DNA-binding protein, HMGB1 (high mobility group box protein 1) may be involved in the transcription and stability of BDV on chromatin by increasing the stability of the viral phosphoprotein (P) on chromatin-bound RNP. Our results show that bornaviruses establish a life cycle highly associated with the cellular chromosome and take advantage of chromosomal stability and dynamics to ensure the integrity of its RNP in the infected nucleus, presenting an alternative fashion of infection by non-reverse

transcribing RNA viruses in eukaryotic cells.

RESULTS

BDV generates viral factories associated with chromatin structures.

To determine how bornaviruses establish stable infection in the nucleus, we first examined the intranuclear distribution of BDV in infected human oligodendroglioma (OL) cells. We performed immunofluorescence analysis (IFA) using antibodies to BDV N and P, both of which are major components of the viral RNP. The viral nucleocapsid is composed of the vRNA tightly encapsidated by N to form the RNP, which serves as the template for replication by the viral polymerase complex, including P (Hock et al., 2010; Schwemmle et al., 1998). IFA showed that BDV N and P colocalize in subnuclear dots, which are usually multiple and variable in size, in the interphase nuclei (Figure 1A). These nuclear dots were seen in almost all infected cells and no known nuclear speckles were found to colocalize with these viral dots (data not shown). Each RNP component alone appears insufficient to assemble such nuclear aggregates (data not shown). Confocal microscope images show that the viral speckles, including granular dots (arrowheads), are localized in contact with the borders of heterochromatin stained by 4',6'-diamidino-2-phenylindole (DAPI) (Figure 1A, insets). Detailed observation with a higher magnification showed that the larger dots form a ring-shaped structure, which may be seen as a hollow spheroid using maximum *z* projections of vertical slices of confocal images (Figure 1B). The intensity profile indicated that the spheroidal body interacts with heterochromatin, mostly at the termini of the structures (Figure 1B). Fluorescence *in situ* hybridization (FISH) using BDV-specific riboprobes showed that

both sense and antisense viral RNAs generate the dot-like and granular speckles in association with DAPI staining in the nucleus (Figure 1C). Interestingly, FISH combined with IFA using anti-N antibody showed that riboprobes hybridized mostly in the cavities of the spheroids (Figure 1D). Considering that the encapsidated vRNA could not be hybridized by riboprobes, the non-encapsidated and/or the nascent vRNA might be inside the cavity. These observations support earlier suggestions (Chase et al., 2007; Schneider et al., 2003) that the BDV-specific dot structure may be a viral factory, in which essential events of the viral replication cycle take place. Furthermore, the viral dot structure may be also unique as a subnuclear speckle, in which RNA transcription may occur, and therefore we called them vSPOT (viral speckle of transcripts).

To further investigate the detailed distribution and ultrastructure of vSPOT in the nucleus, we performed correlative fluorescence microscopy-electron microscopy (FM-EM) and immuno-EM analyses. The correlative FM-EM technique allowed us to determine the localization of viral factories by both FM and EM in the same samples. BDV-infected cells were stained with anti-N antibody and DAPI and examined under FM, and the same fields were observed under EM. As shown in Figures 2A and S1A, in interphase cells, vSPOT was observed as a highly electron-dense, spherical aggregate without a membrane, which often contained a low density cavity in the center (Panel 2). The high magnification images showed that vSPOT is composed of a complex of twisted filamentous structures, which often show helical shapes (Panel 3, arrows) and seem to be connected to the surrounding chromatin structures, such as highly electron-dense heterochromatin (Panel 2, arrowheads), directly or by thin fibrils (Panel 4, arrows). Serial section analysis showed that heterochromatin

territories are closely associated with vSPOT (Figure 2B, arrowheads). Furthermore, immuno-EM analysis using anti-N antibody revealed that the signals of N are mainly found at the rim of vSPOT (Figures 2C and S1B) and also can be detected in close contact with heterochromatin as small aggregates (Figure 2D, arrow). These observations were consistent with the immunofluorescence images shown in Figure 1 and indicated that BDV may use the chromatin structure as a scaffold for assembly of viral factories in the interphase nuclei.

BDV RNP is tethered to mitotic chromosomes.

BDV can persistently infect not only non-dividing neurons but also dividing cells (Brnic et al., 2012; Okamoto et al., 2003), and previous reports suggested chromatin-association of BDV (Suberbielle et al., 2008; Tomonaga, 2007). Thus, we next investigated in detail the localization of BDV RNP during the phases of mitosis by both IFA and EM analysis. During the metaphase stage of mitosis, in which the nuclear membrane breaks down and the chromosomes are highly condensed in the center of cells, vSPOTs disappeared and the RNP proteins seemed to be widely dispersed on the surfaces of the condensed chromosomes (Figures 3 and S2A). The maximum *z* projections of vertical slices of confocal images revealed that small granules were tethered to the metaphase chromosome. Furthermore, during anaphase and telophase, in which the divided chromosomes move apart toward the poles of the spindle, the fluorescence was shown to associate mostly with the separating chromosomes (Figures 3 and S2A). Recombinant N labeled with fluorescent proteins also localized to mitotic chromosomes in the living infected cells (Figure S2B), suggesting that the interaction between BDV proteins and mitotic chromosomes is not an artifact generated by

cell fixation. Furthermore, we also observed distribution of vRNA on mitotic chromosomes by FISH. The fluorescence for vRNA was clearly detected on metaphase chromosomes of BDV-infected cells, although the signal appeared to be weak, probably due to the tight encapsidation of vRNA on mitotic chromosomes (Figure 3B).

We also performed correlative FM-EM analysis using the metaphase and anaphase stages of BDV-infected cells. During metaphase, fluorescence clearly corresponded to the highly electron-dense structures, which could be seen as tangles of coiled electron-dense threads (Figure 4A, panels 1 and 2). The structures seemed to be tethered to the metaphase chromatin by a thin network of chromatin fibrils (Figure 4A, panels a to d). Serial sectioning revealed that the highly electron-dense tangles are spherically shaped with a diameter of less than 500 nm, suggesting that they may consist of only a small number of RNPs (Figure S3). The immune-EM analysis revealed that anti-N antibody reacted with the tangles on the condensed chromatin of metaphase cells (Figure 4B). In anaphase cells, although the fluorescence seemed to correspond to highly electron-dense aggregates on the separating chromosomes (Figure 4C, arrowheads), an RNP-like structure, which can be obviously distinguished from the condensed chromosomes, was not seen by correlative FM-EM analysis. On the other hand, the immune-EM analysis clearly showed that N was dispersed on the telophase chromosomes (Figure 4D). All these results suggest that BDV interacts directly with mitotic chromosomes and is segregated into the daughter cell nuclei along with the separating chromosomes, which might ensure the continued intranuclear residence of BDV during persistent infection.

Replication-competent BDV RNP associates with the host chromosome.

By microscopic analyses, we showed that BDV RNP components associate with the host chromosome throughout the cell cycle. On the other hand, it is still not clear whether the fluorescence on chromatin consists of infectious BDV RNP. To determine whether BDV actually interacts with chromatin as an RNP, we first carried out a chromatin-binding assay using both asynchronous and metaphase-arrested BDV-infected OL cells. We isolated chromatin fractions from the same numbers of asynchronous and metaphase cells and released chromatin-bound factors using micrococcal nuclease (MNase). As shown in Figure 5A, the MNase-resistant encapsidated vRNA, as well as BDV N and P, was detected at a similar level in the chromatin-binding fraction from both asynchronous and metaphase-arrested cells. Considering that P stably associates with chromatin only via interaction with N (Figure 5B), this result indicated that BDV interacts with chromatin as a form of RNP containing P. Furthermore, the fact that the asynchronous culture contains less than 10% mitotic cells suggests that relatively the same amount of RNP is associated with chromatin, regardless of the stage of the cell cycle. Salt-extraction of chromatin-associated proteins indicated that RNP components are released from chromatin with similar kinetics and are mostly extracted by 200 mM salt (Figure S4A), indicating a tight affinity of RNP for cellular chromatin. Moreover, we also found that transfection of the chromatin-binding fraction from both asynchronous and metaphase-arrested BDV-infected OL cells into uninfected cells led to viral replication (Figure 5C). All these data indicated that replication-competent BDV RNP is associated with the cellular chromosome throughout the cell cycle.

BDV RNP interacts with chromatin via core histones.

We sought next to determine the binding partner of N on chromatin by an immunoprecipitation assay using BDV-infected OL cells transfected with tandem-affinity-purification-tagged N (TAP-N). SDS-PAGE followed by mass spectrometry revealed that TAP-N interacts with poly(adenosine diphosphate-ribose) polymerase 1 (PARP-1), a nucleosome binding, non-histone protein, as well as core histones (Figure S4B). The specificity of the analysis was verified by western blotting (Figure S4C). Unexpectedly, these proteins could not be precipitated from uninfected cells transfected with TAP-N only. As shown in Figure 5B, the chromatin-binding ability of TAP-N seems to be markedly low when compared with wild-type N, suggesting that the TAP-tag may interfere with the direct binding of the fusion protein to chromatin. On the other hand, TAP-N may be able to associate with chromatin by being incorporated into the viral nucleocapsid in infected cells. The interaction of viral RNP with core histones was confirmed by immunoprecipitation analysis using anti-N antibody. The core histones, as well as BDV P and MNase-resistant vRNA, were clearly immunoprecipitated from the chromatin-binding fractions from both asynchronous and metaphase-arrested BDV-infected cells (Figure S4D). Altogether, these results suggest that core histones may provide a platform for BDV RNP on chromatin. Note that PARP-1 appeared to not colocalize with vSPOT in the infected nucleus (Figure S4E). Considering that PARP-1 is a mobile and abundant nuclear chromatin-associated protein, it might be possible that PARP-1 associates with N outside of vSPOT.

HMGB1 regulates BDV RNP activity in the interphase nucleus.

We investigated next how the activity of viral RNP is regulated in the nucleus. To this end, we focused on the chromatin-binding, DNA architectural protein, HMGB1, which has been demonstrated to directly bind to P (Kamitani et al., 2001; Zhang et al., 2003). BDV P is a scaffold protein for assembly of the viral polymerase complex and, therefore, HMGB1 is likely a key regulator of RNP activity. In fact, we found that HMGB1 is clearly incorporated into vSPOT in infected cells (Figure 6A). HMGB1 is a highly mobile protein in the nucleus and its mobility may be required for effective modulation of DNA structure (Bianchi and Agresti, 2005; Catez and Hock, 2009). To understand the involvement of HMGB1 in RNP activity, we first investigated the movement of HMGB1 in vSPOTs in living cells. The movement of enhanced green fluorescent protein (EGFP) fused with HMGB1 was analyzed by fluorescence recovery after photobleaching (FRAP) and fluorescence loss in photobleaching (FLIP) analyses in living BDV-infected cell nuclei. In FRAP, an area including a vSPOT was bleached and recovery of the fluorescence signal in that vSPOT was monitored. As shown in Figure 6B, fluorescence recovered rapidly in bleached vSPOTs in the nuclei of EGFP-HMGB1-transfected cells. In FLIP analysis, repeated photobleaching of vSPOTs in the nuclei of cells transfected with EGFP-HMGB1 led to an overall loss of fluorescence from the nuclei, including from unbleached vSPOTs (Figure 6B). The FRAP/FLIP analysis of EGFP-HMGB1 was also monitored in chromatin areas other than vSPOT sites in BDV-infected and uninfected nuclei, demonstrating similar movement of HMGB1 between infected and uninfected nuclei (Figure S5A). In contrast, FRAP analysis using EGFP-N-transfected, BDV-infected cells revealed that fluorescence in bleached vSPOTs only recovered to the background level during the monitoring time, indicating that

EGFP-N molecules in bleached vSPOTs are not replaced by unbleached EGFP-N (Figure 6B). Furthermore, the fluorescence remained in unbleached vSPOTs during the 300 s bleaching period in cells expressing EGFP-N in FLIP (Figure. 6B, arrowhead). These observations indicated that N is considerably immobile in the vSPOT, while HMGB1 enters and leaves the vSPOTs repeatedly in a brief period.

To understand the role of the interaction between BDV P and HMGB1 in the viral life cycles, we generated recombinant BDV mutants expressing BDV P variants with severely impaired HMGB1 binding activity. Alanine-scanning mutagenesis within the HMGB1-binding site of BDV P revealed that substitution of amino acid 84 reduces its efficiency to bind HMGB1 in the mammalian-two-hybrid system significantly and affects its polymerase cofactor activity in the BDV minireplicon assay (Figure S5B). Two alternative substitutions in which the glutamate residue in position 84 was substituted with either asparagine or glutamine resulted in BDV P mutants, P-E84N and P-E84Q, which failed to bind to HMGB1 efficiently, but displayed unimpaired polymerase cofactor activity. Biochemical binding assays confirmed the strongly impaired binding capacity of the two BDV P mutant proteins to HMGB1 (Figure S5C). The recombinant viruses, rBDV-E84N and rBDV-E84Q, were successfully recovered by reverse genetics technique (Figures 6D and 6E), although colocalization of HMGB1 with vSPOT was not found in cells infected with the mutant viruses (Figure 6C). It was observed, however, that the spread of both viruses was impaired and severely attenuated in OL cells (Figures S5D). Interestingly, after several passages, subsequent sequence analysis identified a lysine to glutamate exchange at position 77 of P-E84N, which partially recovered its binding capacity to HMGB1 (Figure 6F). Based

on these results, we speculated that the binding of HMGB1 with BDV P may be retained for efficient propagation and persistent infection in cultured cells.

To understand the involvement of HMGB1 in persistent BDV infection in more detail, we generated small-interfering RNA (siRNA) and lentiviral short hairpin RNA (shRNA) vectors to knockdown the expression of HMGB1 of persistently BDV-infected cells. Because HMGB1 is an abundant nuclear protein (Catez and Hock, 2009; Stros, 2010) and it was very difficult to obtain completely knocked-down cells, we generated BDV-infected OL cells stably expressing shRNA, in which expression of HMGB1 was reduced to 70 to 90% that of normal cells (Figure S6A). The reduced levels of HMGB1 did not induce apoptotic cell death (data not shown), indicating there was no severe chromosomal instability in the knockdown cells. The structure of vSPOT appeared to be unaffected by the knockdown of HMGB1 (Figure S6B). In transient HMGB1-knockdown cells, interestingly, chromatin-associated levels of P were reduced markedly, although the amount of N was comparable in control and knockdown cells (Figure 7A). The total cellular level of P, as well as N, was not changed by the knockdown of HMGB1 (Figure 7B). To rule out the possibility of an off-target effect of shRNA, we generated HMGB1-Escape, in which silent mutations were introduced into the shRNA target sequences. Expression of HMGB1-Escape, but not of a control empty plasmid, led to a recovery in the level of P on chromatin in knockdown cells (Figure 7A). The observation that P alone cannot interact with chromatin suggested that HMGB1 is involved in the interaction or stability of P in chromatin-bound RNP.

To investigate whether the reduced interaction of P with RNP following HMGB1-knockdown in persistently BDV-infected cells exerts adverse effects on the

persistent infection of BDV, we estimated the infection ratio, as well as transcription level, of BDV after HMGB1 knockdown in the persistently infected cells, in which infection rate was almost 100% before the knockdown. As shown in Figure 7C, the infection ratio gradually decreased in the HMGB1-knockdown cell lines. Furthermore, to understand whether HMGB1-knockdown affects BDV RNA transcription in the persistently infected cells, we determined the relative amount of BDV mRNA to vRNA. The knockdown significantly reduced the transcription level to 20 to 50% of that of the control cells during the cultured period (Figure 7D). We also confirmed that BDV polymerase activity was significantly reduced in the cells treated with siRNA for HMGB1 by the minireplicon assay (Figures S6C and S6D).

We next performed a pulse-chase experiment by labeling cells with [^{35}S]-methionine/cysteine, followed by a chase with growth medium. A chromatin-binding fraction was prepared from HMGB1-knockdown cells and immunoprecipitated with anti-N antibody. The input chromatin-binding fraction level was normalized relative to the core histones. Consistent with the above results, the RNP-associated level of P was markedly reduced in the HMGB1-knockdown cells (Figure 7E). Interestingly, the level of chromatin-bound N appeared to decrease rapidly in the knockdown cells during the chase period, whereas chromatin-bound N appeared to be relatively stable in the control cells. The half-life of chromatin-bound N was estimated to be 9.66 ± 1.34 h and 4.28 ± 0.051 h in control and knockdown cells, respectively (p <0.005) (Figure 7E), suggesting that the knockdown of HMGB1 reduces the stability of chromatin-bound RNP. Moreover, we investigated the association of BDV RNP with mitotic chromosomes of HMGB1-knockdown

cells. Intriguingly, association of RNP with mitotic chromosomes was markedly abolished in the stable knockdown cells, especially in Hmg-Kd2 cells (Figures 7F, S6E and S6F). Taken together, these data strongly suggested that HMGB1 may endow the efficient transcription and stability of BDV RNP on chromatin, leading to the maintenance of the persistent infection in the nucleus.

DISCUSSION

This report illustrates the detailed dynamics of intranuclear infection by an RNA virus in eukaryotic cells. Our results using microscopic analyses revealed that BDV generates various-sized spheroidal aggregates containing both sense and antisense viral RNAs in the nucleus and therefore is considered to be the viral factory. The morphology and functions of the viral factories of mononegaviruses have been studied in detail for rabies virus (Lahaye et al., 2009; Menager et al., 2009). Inclusion bodies (IBs) are known to form in the cytoplasm of cells infected with rabies virus, which show similar characteristics to the Negri bodies found in the nerve cells in infected brains. Recently, Lahaye et al. (2009) demonstrated that IBs are spherical in shape and often have a cavity in the center, which contains the viral RNA. It was also shown that rabies virus IBs appear to be surrounded by N and P proteins. These morphological similarities between rabies IBs and BDV vSPOTs may represent the structural commonality of viral factories of mononegaviruses to synthesize and/or mature de novo viral RNAs. On the other hand, while rabies IBs have been shown to be associated with a double membrane in the cytoplasm, BDV vSPOTs are not segregated by a membrane structure. This difference may be attributable to how they interact with cellular factors or the

microenvironment, in addition to the specificity of the replication site. In fact, EM analyses revealed that vSPOTs seem to be closely associated with chromatin structures, such as condensed heterochromatin and chromatin fibrils (Figure 2). These observations suggested a dynamic interaction between the viral factory and intranuclear factors, including chromatin environments, in the interphase nuclei.

During mitosis, BDV RNP showed a unique distribution in the nucleus. At the beginning of mitosis, BDV RNP was dispersed diffusely on the condensed metaphase chromosomes (Figure 3). The EM analyses demonstrated that the RNP-like coiled structures seem to be present on the chromosomes intertwined with condensed mitotic chromatin (Figure 4). More striking was the observation that RNP is seemingly segregated into the daughter cell nuclei along with the mitotic chromosomes. The chromatin-binding assay, as well as the RNP transfection analysis, strongly supported the concept that a replication-competent BDV RNA interacts with chromatin throughout the cell cycle (Figure 5). Considering that almost all cellular nuclear RNPs, including small nuclear RNPs and heterogeneous nuclear RNPs, leave the nucleus prior to mitosis and reenter the daughter cell nuclei at the end of the mitotic process (Calado and Carmo-Fonseca, 2000; Friend et al., 2008; Prasanth et al., 2003), BDV RNP may be a unique nuclear RNP that behaves like a component of cellular chromosomes in infected cells.

Although BDV is known as a neurotropic virus, astrocytes can also be infected with BDV and play important roles in the viral life cycle (Carbone et al., 1991). In addition, it has recently been demonstrated that neuronal progenitor cells are also a target of BDV in the brain (Brnic et al., 2012). More importantly, vertical transmission of BDV was demonstrated in

both natural and experimental infection, and BDV antigen was detected in decidual cells and endodermal cells of the infected placenta (Hagiwara et al., 2000; Okamoto et al., 2003). These observations indicated that non-neuronal and undifferentiated cells may be important targets for BDV infection. We also have recently found endogenous bornavirus elements in many mammalian genomes, suggesting that bornaviruses may infect germline cells (Horie et al., 2010). Thus, the segregation of the BDV genome into daughter cell nuclei in association with mitotic chromosomes could be a highly-evolved strategy for an RNA virus to ensure spatial stability and maintain persistent residence in the nucleus.

Previous studies revealed that latent DNA viruses, such as Kaposi's sarcoma-associated herpesvirus (KSHV), Epstein-Barr virus and papillomaviruses, maintain their genomes in the nucleus as multicopy episomes tethered to host mitotic chromosomes (Ballestas et al., 1999; Feeney and Parish, 2009; Lehman and Botchan, 1998; Piolot et al., 2001) and that chromosomal proteins, including core histones, are involved in the binding of the viral DNAs with cellular chromosomes. It has been reported that KSHV's LANA, which mediates viral episome attachment to mitotic chromosomes, directly binds to core histone H2A/2B (Barbera et al., 2006; Krithivas et al., 2002). Furthermore, papillomavirus E2 proteins have been shown to bind to Brd4, which associates with acetylated histone H4, to anchor the viral DNA to chromosome (You et al., 2004). In this study, interestingly, we also found that BDV RNP interacts with core histones and PARP-1, a non-histone, chromatin-associated protein, on chromatin. These observations imply that nucleosomes play important roles as a docking platform for the genomes of chromatin-associated viruses and that tethering viral genomes with host chromosomes could be a good way to maintain the presence of the virus within the

nuclear envelope.

In this study, we showed that the non-histone, DNA architectural protein, HMGB1, may affect the transcription, as well as stability, of BDV on chromatin via interaction with P (Figures 6 and 7). HMGB1 is an extremely mobile protein in the nucleus and binds to chromatin for less than a few seconds to modulate the structure of DNA (Bianchi and Agresti, 2005; Catez and Hock, 2009). Furthermore, this protein has been shown to interact with many transcriptional proteins to stabilize their binding to cognate DNA sites (Muller et al., 2004). HMGB1 is known to be a multifunctional nuclear protein widely involved in the chromosomal maintenance of host cells. A well-studied nuclear factor regulated by HMGB1 is the glucocorticoid receptor (GR), a transcriptional protein which binds to and releases from chromatin in cycles of only a few seconds (Agresti et al., 2005; Bianchi and Agresti, 2005). Remarkably, it is known that such a fleeting interaction is sufficient to induce large-scale remodeling of chromatin and promote transcriptional activation. HMGB1 has been shown to increase the stability of GR on the promoter sites by direct interaction with chromatin and cooperatively control the transcription activity of GR (Agresti et al., 2005). We found that HMGB1 distributes instantaneously and repeatedly to vSPOTs and then increases the association of P with RNP (Figures 6 and 7). This seems to be very similar to the regulation of GR. Given that HMGB1 can modify chromatin structure by interacting with it for less than a few seconds (Bonaldi et al., 2002; Phair et al., 2004), it is highly likely that such a brief association of HMGB1 with vSPOTs is sufficient to play a role in RNP activity on chromatin. Interaction with HMGB1 might endow the stability of P on the RNP on chromatin, resulting in efficient viral transcription. Our data using rBDVs and HMGB1-knockdown cells strongly

support this hypothesis.

Our study revealed that BDV is an RNA virus with a life cycle closely associated with host chromosomes. BDV may take advantage of the chromosomal stability and dynamics to ensure its own transcription and persistence in the nucleus. In fact, a previous study using a proteomic analysis has revealed that histone modifications, such as H2B acetylation on Lys-5, are found in the BDV-infected primary cortical neurons (Suberbielle et al., 2008). This finding suggests that BDV might directly modify the epigenetic environment of the chromatin surrounding the sites of the viral RNP to ensure efficient viral genome survival or persistent infection. Further understanding of the infection and replication of BDV on chromatin may provide not only details of a yet unexplored interaction between viruses and eukaryotic cells, but also alternative mechanisms of the pathogenesis of an animal RNA virus.

EXPERIMENTAL PROCEDURES

Cell lines and virus

The OL cell line, derived from a human oligodendroglioma, was cultured in Dulbecco's modified Eagle's medium (DMEM)-high glucose (4.5%) supplemented with 5% fetal bovine serum (FBS) and 4 mM glutamine. HEK293T (293T; human embryonic kidney), Vero (African green monkey kidney) and C6 (rat glioma) cells were cultured in DMEM-low glucose (1.0%) supplemented with 5% FBS. BDV-infected OL cells, a cell line persistently infected with strain huP2br (Nakamura et al., 2000), were cultured using the same conditions as the parental cell line. The shRNA expression cell clones were cultured in DMEM-high

glucose supplemented with 2 µg/ml puromycin.

Correlative FM-EM

For observation by FM-EM, BDV-infected and -uninfected OL cells were cultured on gridded, 35 mm glass-bottom dishes (Mat Tek) in 1 ml of DMEM at 37°C overnight. Cells on the grid were fixed and stained with the specific antibodies as described above and then examined using a confocal laser scanning microscope. The same specimens were then further incubated with 2.5% glutaraldehyde and 2% formaldehyde in PBS at 4°C overnight. After three washings with PBS, the samples were post-fixed with 1% osmium tetroxide and 0.5% potassium ferrocyanide in PBS for 1 h, washed with distilled water three times, dehydrated in ethanol, and embedded in Epon812 (Structure Probe). Ultrathin sections of the cell (70-nm thick) were stained with saturated uranyl acetate and Reynolds lead citrate solution. The electron micrographs were taken with a JEOL JEM-1011 transmission electron microscope (JEOL, Ltd.).

Chromatin isolation

To isolate chromatin, cells (1×10^7 cells) were resuspended in 300 µl buffer A (10 mM HEPES, pH 7.9, 10 mM KCl, 1.5 mM $MgCl_2$, 0.34 M sucrose, 10% glycerol, 1 mM DTT, complete protease inhibitor [Roche]) containing 0.1% Triton X-100. After incubation for 10 min on ice, nuclei were collected in a pellet by centrifugation (5 min, 1,200 × *g*, 4°C). Nuclei were washed three times with buffer A and lysed in buffer B (3 mM EDTA, 0.2 mM EGTA, 1 mM DTT, complete protease inhibitor) for 30 min on ice. The chromatin enriched pellet was

collected by centrifugation (5 min, 1,700 × *g*, 4°C) and the supernatant was removed to yield a nucleosolic fraction. The pellet was washed twice with buffer B and once with MNase buffer (10 mM Tris-HCl, pH 8.0, 5 mM NaCl, 2.5 mM $CaCl_2$) and resuspended in 200 µl MNase buffer containing 20 U MNase. After incubation for 5 min at 37°C, the MNase reaction was stopped by the addition of an EDTA-EGTA solution to a final concentration of 5 mM, and then the supernatant was collected by centrifugation (5 min, 2,000 × *g*, 4°C) as a chromatin-binding fraction. The pellet was washed three times with MNase buffer and collected as an insoluble fraction. To separate the chromatin into euchromatin and heterochromatin, nucleic were resuspended in 200 µl buffer A containing 2.5 mM $CaCl_2$ and 20 U MNase and incubated for 4 min at 37°C. After centrifugation (5 min, 5,000 × *g*, 4°C), the supernatant was removed to yield a euchromatin fraction. The pellet was washed three times and then lysed with 200 µl buffer B for 15 min on ice. After centrifugation (5 min, 5,000 × *g*, 4°C), the supernatant was removed to yield a heterochromatin fraction.

FRAP and FLIP assays

Cells grown on 35 mm diameter glass-base dishes were transfected with EGFP fused HMGB1 or BDV N with LipofectamineTM 2000 (Invitrogen). At 20-28 h post-transfection, the medium was replaced with pre-warmed alpha-MEM (Gibco). Photobleaching experiments were carried out with a Digital Eclipse Spectral Imaging Confocal Laser Microscope C1si (Nikon Inc.). FRAP assays were done with a confocal laser-scanning microscope FV1000 (Olympus Inc.) using the 473-nm laser line of a semiconductor laser. Briefly, three pre-bleach images were acquired, followed by a single bleach pulse of 450 ms using a 1.4 µm diameter

beam spot. Single images were then collected with a 0.57 s interval. The laser power was set to 5% for imaging and 90% for bleaching. Total fluorescence was determined for each image and compared to the initial total fluorescence to determine the amount of fluorescence lost during bleaching and imaging. The fluorescence intensity in the bleached area was normalized to the initial fluorescence in the bleached area. Each experiment was repeated at least three times, each of which involved observation of at least 15 independent cells.

shRNA expression

Lentivirus plasmids for shRNA expression (pLKO.1puro) were purchased from Sigma-Aldrich. Five independent shRNA sequences for HMGB1 were determined from a lentiviral vector-based shRNA library, Mission shRNA (Sigma-Aldrich). To generate shRNA expression lentiviral vectors, plasmids were co-transfected into 293T cells and the medium was changed 24 h post-transfection. Culture supernatants containing lentiviral vectors were collected at 48 h post-transfection, filtered through a 0.45-μm filter. To determine the titer of lentiviral vectors, OL cells were infected with serial dilutions of the viruses, cells were selected with puromycin, and the number of colonies was counted. To establish HMGB1-knockdown, BDV-infected cell lines, Hmg-Kd1, Hmg-Kd2 and Hmg-Kd3, BDV persistently infected OL cells were infected with lentiviral vectors encoding shRNA for HMGB1. The lentivirus vector-infected cells were selected with puromycin and cloned by limiting dilution. After establishment of HMGB1-knockdown, BDV persistently infected cell lines, the infectious ratio and the levels of viral RNAs were monitored by immunofluorescence assay using anti-N antibody and quantitative real-time RT-PCR.

ACKNOWLEDGEMENTS

We thank Dr. K. Saito of DNA-chip Development Center for Infectious Diseases (RIMD, Osaka University) for mass spectrometry analysis. This study was supported in part by Funding Program for Next Generation World-Leading Researchers (NEXT program) from Japan Society for the Promotion of Science (JSPS) (KT), Grants-in-aid for Scientific Research on Priority Areas (Infection and Host Responses; Matrix of Infection Phenomena) from Ministry of Education, Culture, Sports, Science and Technology (MEXT) (KT) and PRESTO from Japan Science and Technology Agency (JST) (KT) and the Deutsche Forschungsgemeinschaft (DFG-SCHW632-/10-2).

REFERENCES

Agresti, A., Scaffidi, P., Riva, A., Caiolfa, V.R., and Bianchi, M.E. (2005). GR and HMGB1 interact only within chromatin and influence each other's residence time. Mol. Cell. *18,* 109-121.

Ballestas, M.E., Chatis, P.A., and Kaye, K.M. (1999). Efficient persistence of extrachromosomal KSHV DNA mediated by latency-associated nuclear antigen. Science *284,* 641-644.

Barbera, A.J., Chodaparambil, J.V., Kelley-Clarke, B., Joukov, V., Walter, J.C., Luger, K., and Kaye, K.M. (2006). The nucleosomal surface as a docking station for Kaposi's sarcoma herpesvirus LANA. Science *311,* 856-861.

Belyi, V.A., Levine, A.J., and Skalka, A.M. (2010). Unexpected inheritance: multiple integrations of ancient bornavirus and ebolavirus/marburgvirus sequences in vertebrate genomes. PLoS Pathog. *6,* e1001030.

Bianchi, M.E., and Agresti, A. (2005). HMG proteins: dynamic players in gene regulation and differentiation. Curr. Opin. Genet. Dev. *15,* 496-506.

Bonaldi, T., Langst, G., Strohner, R., Becker, P.B., and Bianchi, M.E. (2002). The DNA chaperone HMGB1 facilitates ACF/CHRAC-dependent nucleosome sliding. EMBO J *21,* 6865-6873.

Brnic, D., Stevanovic, V., Cochet, M., Agier, C., Richardson, J., Montero-Menei, C.N.,

Milhavet, O., Eloit, M., and Coulpier, M. (2012). Borna Disease Virus Infects Human Neural Progenitor Cells and Impairs Neurogenesis. J. Virol. *86,* 2512-2522.

Calado, A., and Carmo-Fonseca, M. (2000). Localization of poly(A)-binding protein 2 (PABP2) in nuclear speckles is independent of import into the nucleus and requires binding to poly(A) RNA. J. Cell Sci. *113,* 2309-2318.

Carbone, K.M., Moench, T.R., and Lipkin, W.I. (1991). Borna disease virus replicates in astrocytes, Schwann cells and ependymal cells in persistently infected rats: location of viral genomic and messenger RNAs by in situ hybridization. J. Neuropathol. Exp. Neurol. *50,* 205-214.

Catez, F., and Hock, R. (2009). Binding and interplay of HMG proteins on chromatin: lessons from live cell imaging. Biochim. Biophys. Acta *1799,* 15-27.

Chase, G., Mayer, D., Hildebrand, A., Frank, R., Hayashi, Y., Tomonaga, K., and Schwemmle, M. (2007). Borna disease virus matrix protein is an integral component of the viral ribonucleoprotein complex that does not interfere with polymerase activity. J. Virol. *81,* 743-749.

Feeney, K.M., and Parish, J.L. (2009). Targeting mitotic chromosomes: a conserved mechanism to ensure viral genome persistence. Proc. Biol. Sci. *276,* 1535-1544.

Friend, L.R., Han, S.P., Rothnagel, J.A., and Smith, R. (2008). Differential subnuclear localisation of hnRNPs A/B is dependent on transcription and cell cycle stage. Biochim. Biophys. Acta *1783,* 1972-1980.

Gonzalez-Dunia, D., Cubitt, B., Grasser, F.A., and de la Torre, J.C. (1997). Characterization of Borna disease virus p56 protein, a surface glycoprotein involved in virus entry. J. Virol. *71,* 3208-3218.

Hagiwara, K., Kamitani, W., Takamura, S., Taniyama, H., Nakaya, T., Tanaka, H., Kirisawa, R., Iwai, H., and Ikuta, K. (2000). Detection of Borna disease virus in a pregnant mare and her fetus. Vet. Microbiol. *72,* 207-216.

Hock, M., Kraus, I., Schoehn, G., Jamin, M., Andrei-Selmer, C., Garten, W., and Weissenhorn, W. (2010). RNA induced polymerization of the Borna disease virus nucleoprotein. Virology *397,* 64-72.

Horie, M., Honda, T., Suzuki, Y., Kobayashi, Y., Daito, T., Oshida, T., Ikuta, K., Jern, P., Gojobori, T., Coffin, J.M., et al. (2010). Endogenous non-retroviral RNA virus elements in mammalian genomes. Nature *463,* 84-87.

Kamitani, W., Shoya, Y., Kobayashi, T., Watanabe, M., Lee, B.J., Zhang, G., Tomonaga, K., and Ikuta, K. (2001). Borna disease virus phosphoprotein binds a neurite outgrowth factor, amphoterin/HMG-1. J. Virol. *75,* 8742-8751.

Krithivas, A., Fujimuro, M., Weidner, M., Young, D.B., and Hayward, S.D. (2002). Protein interactions targeting the latency-associated nuclear antigen of Kaposi's sarcoma-associated herpesvirus to cell chromosomes. J. Virol. *76,* 11596-11604.

Lahaye, X., Vidy, A., Pomier, C., Obiang, L., Harper, F., Gaudin, Y., and Blondel, D. (2009). Functional characterization of Negri bodies (NBs) in rabies virus-infected cells: Evidence that

NBs are sites of viral transcription and replication. J. Virol. *83,* 7948-7958.

Lehman, C.W., and Botchan, M.R. (1998). Segregation of viral plasmids depends on tethering to chromosomes and is regulated by phosphorylation. Proc. Natl. Acad. Sci. USA *95,* 4338-4343.

Menager, P., Roux, P., Megret, F., Bourgeois, J.P., Le Sourd, A.M., Danckaert, A., Lafage, M., Prehaud, C., and Lafon, M. (2009). Toll-like receptor 3 (TLR3) plays a major role in the formation of rabies virus Negri Bodies. PLoS Pathog. *5,* e1000315.

Muller, S., Ronfani, L., and Bianchi, M.E. (2004). Regulated expression and subcellular localization of HMGB1, a chromatin protein with a cytokine function. J. Intern. Med. *255,* 332-343.

Nakamura, Y., Takahashi, H., Shoya, Y., Nakaya, T., Watanabe, M., Tomonaga, K., Iwahashi, K., Ameno, K., Momiyama, N., Taniyama, H., et al. (2000). Isolation of Borna disease virus from human brain tissue. J. Virol. *74,* 4601-4611.

Okamoto, M., Hagiwara, K., Kamitani, W., Sako, T., Hirayama, K., Kirisawa, R., Tsuji, M., Ishihara, C., Iwai, H., Kobayashi, T., et al. (2003). Experimental vertical transmission of Borna disease virus in the mouse. Arch. Virol. *148,* 1557-1568.

Phair, R.D., Scaffidi, P., Elbi, C., Vecerova, J., Dey, A., Ozato, K., Brown, D.T., Hager, G., Bustin, M., and Misteli, T. (2004). Global nature of dynamic protein-chromatin interactions in vivo: three-dimensional genome scanning and dynamic interaction networks of chromatin proteins. Mol. Cell. Biol. *24,* 6393-6402.

Piolot, T., Tramier, M., Coppey, M., Nicolas, J.C., and Marechal, V. (2001). Close but distinct regions of human herpesvirus 8 latency-associated nuclear antigen 1 are responsible for nuclear targeting and binding to human mitotic chromosomes. J. Virol. *75*, 3948-3959.

Prasanth, K.V., Sacco-Bubulya, P.A., Prasanth, S.G., and Spector, D.L. (2003). Sequential entry of components of the gene expression machinery into daughter nuclei. Mol. Biol. Cell *14*, 1043-1057.

Schneider, U. (2005). Novel insights into the regulation of the viral polymerase complex of neurotropic Borna disease virus. Virus Res. *111*, 148-160.

Schneider, U., Martin, A., Schwemmle, M., and Staeheli, P. (2007). Genome trimming by Borna disease viruses: viral replication control or escape from cellular surveillance? Cell. Mol. Life Sci. *64*, 1038-1042.

Schneider, U., Naegele, M., Staeheli, P., and Schwemmle, M. (2003). Active borna disease virus polymerase complex requires a distinct nucleoprotein-to-phosphoprotein ratio but no viral X protein. J. Virol. *77*, 11781-11789.

Schwemmle, M., Salvatore, M., Shi, L., Richt, J., Lee, C.H., and Lipkin, W.I. (1998). Interactions of the borna disease virus P, N, and X proteins and their functional implications. J. Biol. Chem. *273*, 9007-9012.

Staeheli, P., Sauder, C., Hausmann, J., Ehrensperger, F., and Schwemmle, M. (2000). Epidemiology of Borna disease virus. J. Gen. Virol. *81*, 2123-2135.

Stros, M. (2010). HMGB proteins: interactions with DNA and chromatin. Biochim. Biophys.

Acta *1799,* 101-113.

Suberbielle, E., Stella, A., Pont, F., Monnet, C., Mouton, E., Lamouroux, L., Monsarrat, B., and Gonzalez-Dunia, D. (2008). Proteomic analysis reveals selective impediment of neuronal remodeling upon Borna disease virus infection. J. Virol. *82,* 12265-12279.

Tomonaga, K. (2007). [Mechanism of nuclear transport and persistent infection of Borna disease virus]. Tanpakushitsu Kakusan Koso *52 (Suppl 10),* 1168-1174.

Tomonaga, K., Kobayashi, T., and Ikuta, K. (2002). Molecular and cellular biology of Borna disease virus infection. Microbes Infect. *4,* 491-500.

You, J., Croyle, J.L., Nishimura, A., Ozato, K., and Howley, P.M. (2004). Interaction of the bovine papillomavirus E2 protein with Brd4 tethers the viral DNA to host mitotic chromosomes. Cell *117,* 349-360.

Zhang, G., Kobayashi, T., Kamitani, W., Komoto, S., Yamashita, M., Baba, S., Yanai, H., Ikuta, K., and Tomonaga, K. (2003). Borna disease virus phosphoprotein represses p53-mediated transcriptional activity by interference with HMGB1. J. Virol. *77,* 12243-12251.

Figure legends

Figure 1. BDV assembles spherical viral factories supported by chromatin structure.

(A) Confocal microscopic analysis of an interphase nucleus of BDV-infected and uninfected OL cells. BDV generates vSPOT (arrows) and granular speckles (arrowheads) in the nucleus. Cells were visualized by anti-BDV N (red) and anti-BDV P (green) antibodies and DAPI (blue). Magnifications of the boxed areas (1 and 2) are shown on the right. Scale bar, 5 μm. (B) A detailed structure of vSPOT. A maximum z projection of 33 vertical slices (x-z plane) is shown. The intensity profiles at dashed lines are indicated at the right. Red, BDV N; Blue, DAPI. Scale bar, 1 μm. (C) Fluorescence *in situ* hybridization of the viral genome and antigenomic RNAs in the nuclei of BDV-infected and uninfected OL cells. Scale bar, 5 μm. Magnifications of the boxed areas (1 and 2) are shown on the right. (D) Distribution of vRNA in vSPOT. Immuno-RNA fluorescence in situ hybridization using BDV N antibody (red) and riboprobe specific for BDV vRNA (green) was performed and analyzed by confocal microscopy. A maximum z projection of 33 vertical slices (x-z plane) is shown. Scale bar, 1 μm.

Figure 2. Correlative FM-EM and immuno-EM analyses of interphase nuclei of BDV-infected cells.

(A and B) BDV-infected and uninfected OL cells stained by anti-N antibody (red) and DAPI (blue) were analyzed by immunofluorescence microscopy and the same fields were analyzed under EM. Serial section (90 nm) analysis was performed for EM observation (B).

Magnifications of the boxed areas are shown. Arrowheads indicate high electron-dense heterochromatin territories. Arrows in panels 3 and 4 of (A) indicate twisted and helical structures in vSPOT and perichromatin-like fibrils connecting between vSPOT and condensed heterochromatin, respectively. V and Hc indicate vSPOT and heterochromatin areas, respectively. Scale bars are indicated. (C and D) Immuno-EM images of vSPOT (C) and granular speckles (D) in BDV-infected and uninfected cells stained with anti-BDV N antibody. The dark signals are the result of gold labeling. BDV N localizes to the rim of vSPOT (C) and in association with condensed heterochromatin (D, arrow). A magnification of boxed area is shown in the right panel (D). Hc, heterochromatin. Scale bars are indicated. See also Figure S1.

Figure 3. BDV is segregated into daughter cell nuclei along with mitotic chromosomes.

(A) The mitotic stages of BDV-infected OL cells were stained by anti-BDV N (red) and anti-BDV P (green) and DAPI (blue) and analyzed by confocal microscopy. Maximum z projections of 36 vertical slices (z-y plane) at dashed lines and higher magnification of the boxed areas are shown on the right. Scale bar, 5 μm. (B) Fluorescence *in situ* hybridization of the viral genome RNA on the metaphase chromatin of BDV-infected and uninfected OL cells. Scale bar, 5 μm. See also Figure S2.

Figure 4. Correlative FM-EM and immuno-EM analyses of mitotic chromosomes of BDV-infected cells.

(A) Metaphase chromosomes of BDV-infected and uninfected cells were stained by anti-N

antibody (red) and DAPI (blue) and examined by immunofluorescence microscopy. The same fields were then analyzed by EM. Arrowheads (a to d) indicate the condensed chromatin fibers. Magnifications of the boxed are shown. Scale bars in panels a to d are 200 nm. (B) Immuno-EM analysis of metaphase chromosomes of BDV-infected and uninfected cells stained with anti-BDV N antibody. The dark granular signals are the result of gold labeling. BDV N localizes on the condensed metaphase chromosomes (arrowheads). Magnifications of pointed signals are shown. Scale bars in panel 2 and 3 are 200 and 500 nm, respectively. (C) Anaphase chromosomes of BDV-infected cells were stained by anti-N antibody (red) and DAPI (blue) and examined by immunofluorescence microscopy. The same fields were then analyzed by EM. Magnifications of the boxed and pointed area are shown. Arrowheads indicate the high electron-dense structures on mitotic chromosomes. (D) Immuno-EM analysis of anaphase chromosomes of BDV-infected cells stained with anti-BDV N antibody. The dark granular signals are the result of gold labeling. BDV N localizes on the condensed metaphase chromosomes. Magnifications of boxed areas are shown. Scale bar in panel 2, 200 nm. See also Figure S3

Figure 5. Replication-competent BDV RNP interacts with chromatin throughout the cell cycle.

(A) Chromatin binding assay of BDV RNP in asynchronous and metaphase-arrested infected cells. BDV N, P and vRNA were detected in the MNase-treated (+) and untreated (-) fractions by western blotting (BDV N and P, ORC2 and Mek2) or RT-PCR (vRNA). ORC2 (chromatin-associated human protein) and Mek2 (cytosolic kinase) were used as controls for

the fractionation. (B) BDV P associates with chromatin only through the interaction with N. The OL cells were cotransfected with expression plasmids of N, TAP-N and P with indicated combinations. Forty-eight hours posttransfection, western blot analyses were performed with whole cell lysates or chromatin-bound fraction using BDV N and P antibodies. (C) RNP isolated from chromatin-binding fractions of uninfected (a) or BDV-infected (b) asynchronous and metaphase-arrested OL cells were transfected into C6 or Vero cells and BDV replication was detected by staining with anti-BDV P antibody (green). The inset shows a 2 x magnification of infected cells. See also Figure S4

Figure 6. Binding of HMGB1 with BDV P may be necessary for efficient BDV persistence.

(A) Distribution of HMGB1 in the cell nuclei infected with wild-type BDV. BDV-infected OL cells were stained by anti-N antibody (red), anti-HMGB1 (green) and DAPI (blue) and examined by immunofluorescence microscopy. Arrows indicate vSPOT. Magnifications of the boxed area are shown. Scale bar corresponds to 5 μm. (B) FRAP and FLIP analyses of EGFP-fused HMGB1 and BDV N. BDV-infected OL cells expressing EGFP-fused HMGB1 and BDV N were imaged before (t = 0) and during FRAP or FLIP of a vSPOT in the nucleus. Images were taken at the times (s) indicated. Arrows in pre-bleaching images (t = 0) indicate the vSPOTs that were bleached. The bleached spots are indicated by white circles. Images were collected with a 0.57 to 0.60 s interval. Scale bar, 5 μm. (C) HMGB1 is specifically incorporated into vSPOT by binding to BDV P. Distribution of HMGB1 in the cell nuclei infected with wild-type BDV (upper panels) and recombinant BDV (rBDV E84N) (lower

panels), which contains a single amino acid mutation in the binding site of P with to HMGB1. Cells were stained by anti-P antibody (red) and anti-HMGB1 (green). Arrows indicate vSPOT. Magnifications of the boxed area are shown. Scale bar corresponds to 5 μm. (D and E) Rescue of rBDVs encoding P mutant by reverse genetics system. BDV protein (D) and transcription (E) were detected by western and northern blotting in Vero cells producing wild-type (wt) or mutant rBDVs (E84Q and E84N), respectively. (F) Partial recovery of HMGB1 binding of P-E84N by substitution of amino acid 77 with glutamate. BDV P mutant harboring the double mutation K77E and E84N (P-77E/84) was test in the mammalian two-hybrid system for its efficiency to bind to rat HMGB1. Error bars represent + SD. See also Figure S5

Figure 7. HMGB1 is involved in BDV RNP dynamics on chromatin.

(A) HMGB1 was transiently downregulated by transfection with HMGB1-specific siRNA (siHMG) or by infection with lentiviral vectors encoding HMGB1-specific shRNAs (shHMG) in BDV-infected OL cells. Ctrl-siRNA and Ctrl-shRNA denote cells treated with scrambled control siRNA and shRNA, respectively. Nt denotes non-treated, BDV-infected cells. shHMG + Empty and + Escape denote shRNA-HMGB1-knockdown cells transfected with an empty plasmid or with a plasmid encoding an shRNA-escape mutant of HMGB1, respectively. The levels of chromatin-associated BDV N and P, as well as total cellular levels of HMGB1, were determined by western blotting. Core histones were visualized by Coomassie blue as an internal control of the input chromatin-binding fractions. For HMGB1 knockdown by shRNA, two independent lentiviral vectors that encode different shRNA sequences were co-infected into BDV persistently infected OL cells. (B) HMGB1 knockdown did not change the total

cellular level of P. The expression of HMGB1 and BDV proteins was detected in the total lysate of the cells transfected siHMGB1 by western blotting. The asterisk indicates a non-specific band. Tubulin is used as an internal control. (C) The infection ratio of BDV after the knockdown of HMGB1 in BDV persistently infected cells. The infection ratios of HMGB1-knockdown, BDV-infected OL cell lines (Hmg-Kd1, -Kd2 and -Kd3) were monitored by immunofluorescence assay using anti-N antibody at the indicated days after the establishment of each knockdown cell line. The infection ratios of the first monitoring point (day 0) are indicated as 1.0 in each knockdown cell line. (D) The relative amount of BDV mRNA to vRNA in three independent HMGB1-knockdown cell lines (Hmg-Kd1, -Kd2 and -Kd3). The levels of BDV P mRNA and vRNA were analyzed by qRT-PCR analysis at the indicate times and the rates of BDV mRNA to vRNA were determined. (C and D) * $p < 0.05$, ** $p < 0.01$. n.s., no significance. Error bars represent +/- SD. (E) Stability of chromatin-associated BDV N in the presence or absence of HMGB1 was determined by pulse-chase assays. Th(*N*) denotes the N half-life (mean ± standard deviation of three independent experiments). Core histones were visualized by Coomassie blue as an internal control of the input chromatin-binding fractions. (F) Immunofluorescence analysis of anaphase chromosomes of BDV-infected OL cells showed that HMGB1-knockdown abrogated the association of BDV RNPs with separating chromosomes. Two independent of Ctrl-shRNA and Hmg-Kd2 cells are shown. Insets contain a 2.5 x magnification of chromatin areas. Blue indicates DAPI staining of nuclei. Scale bar, 5 μm. See also Figure S6

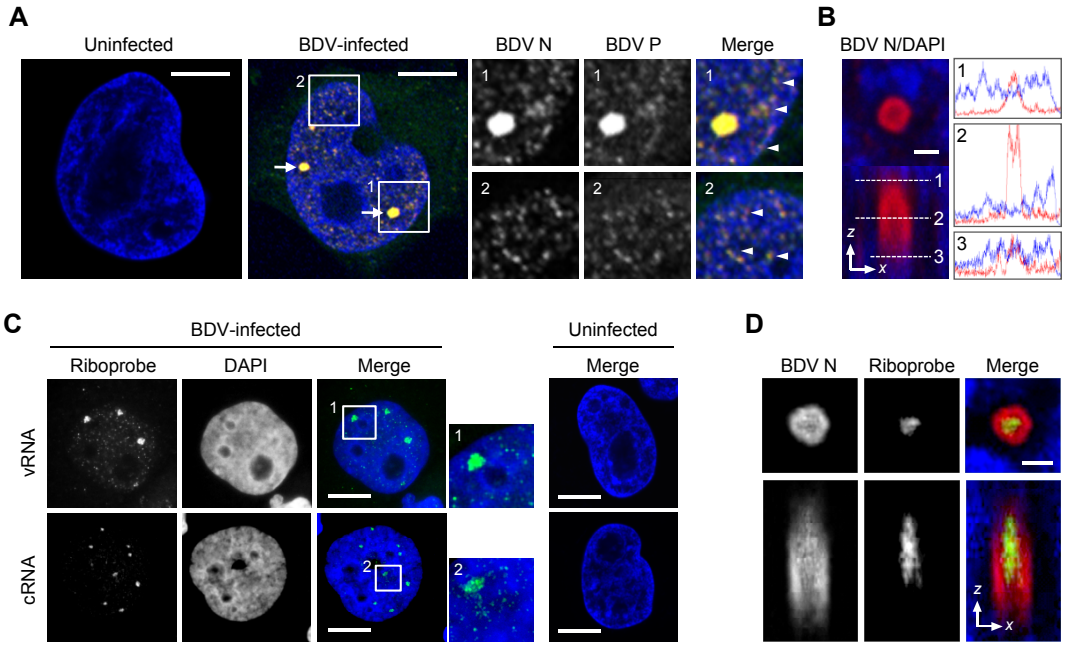

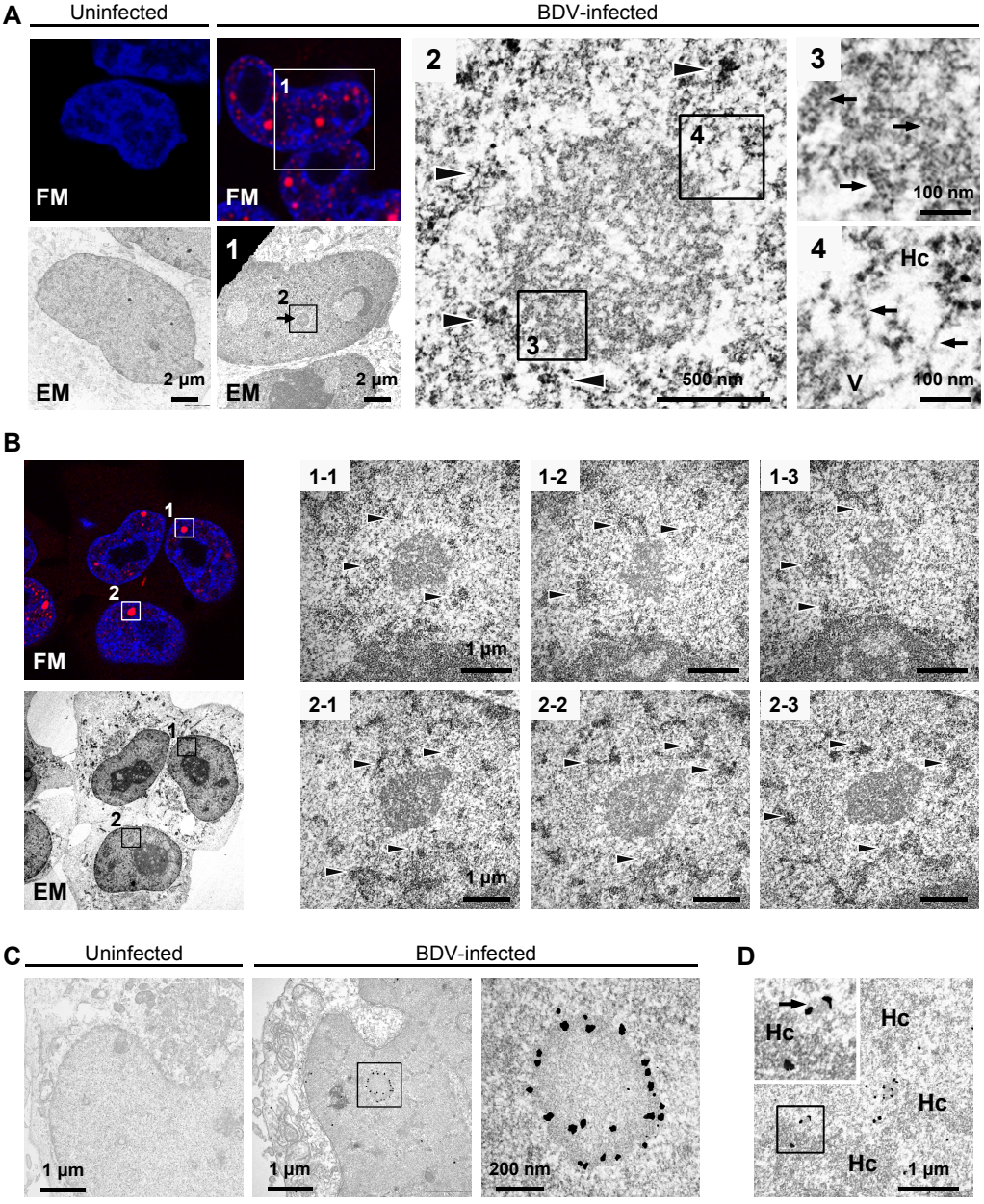

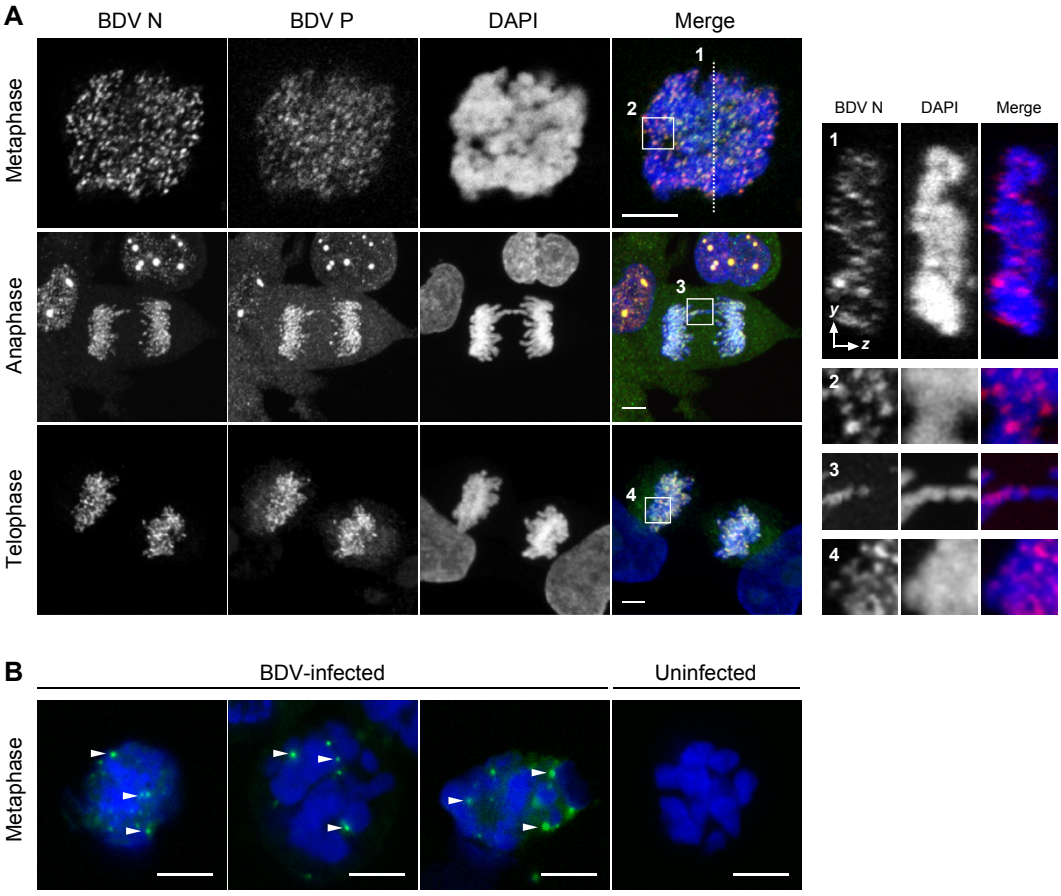

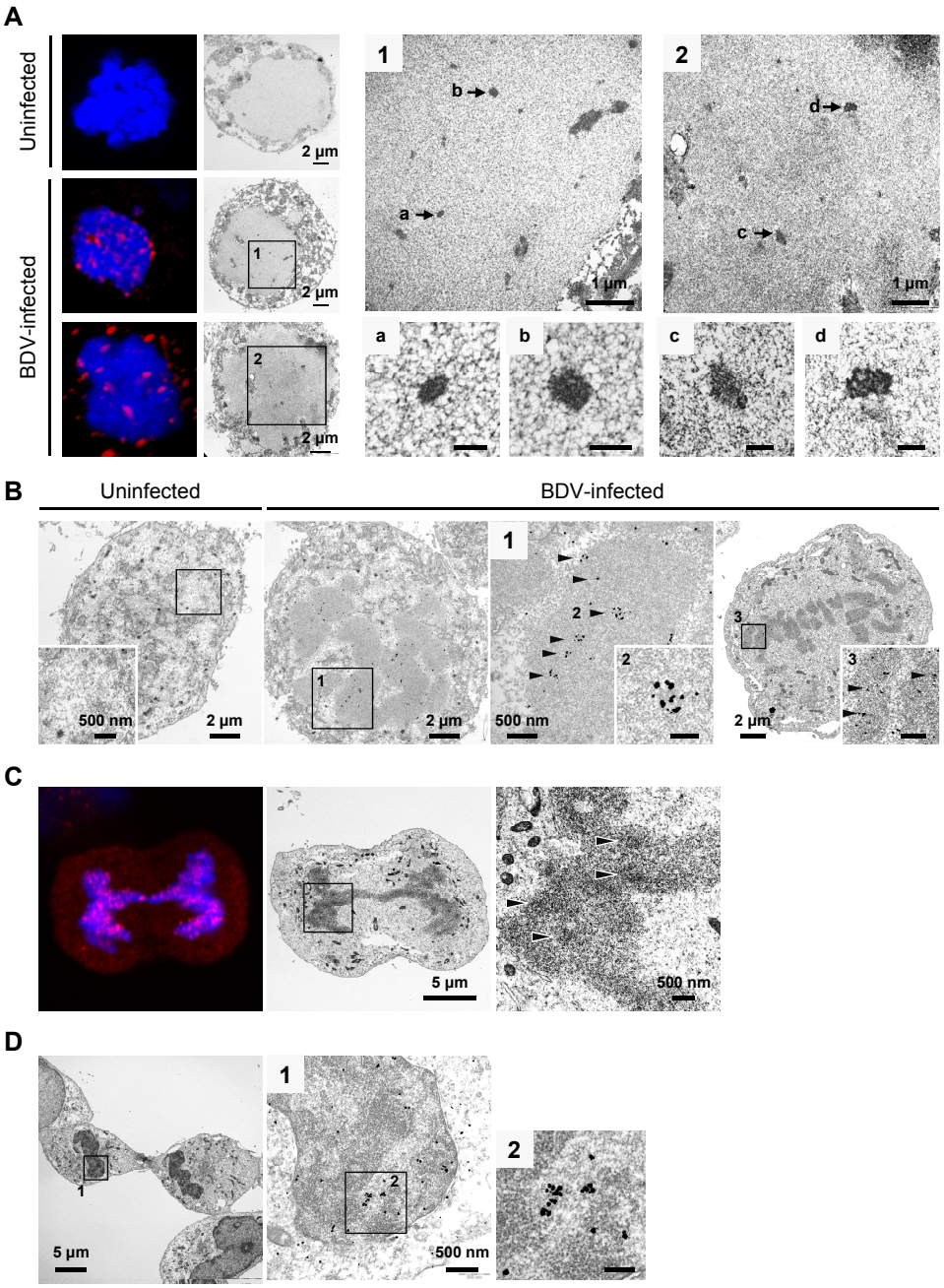

Fig. 5

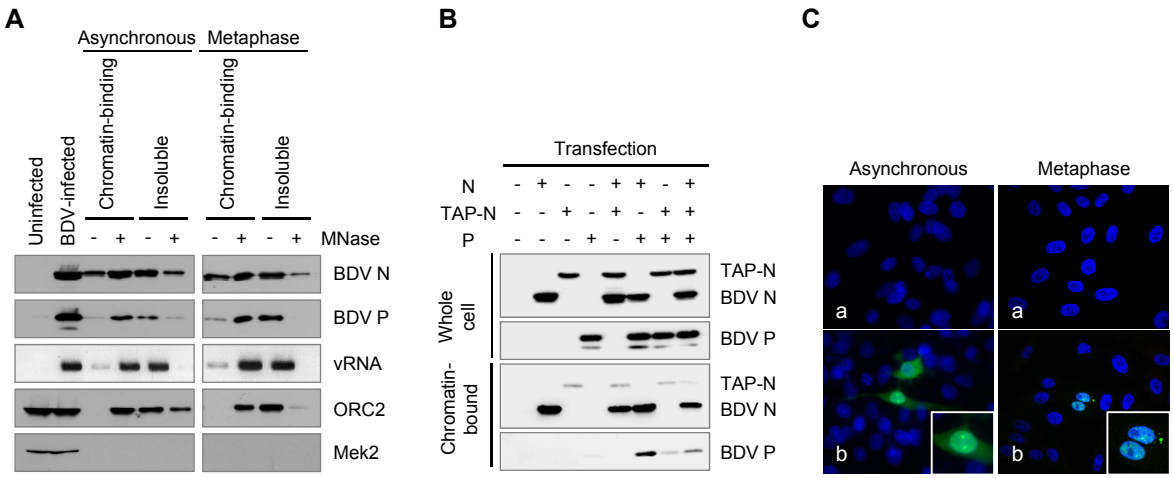

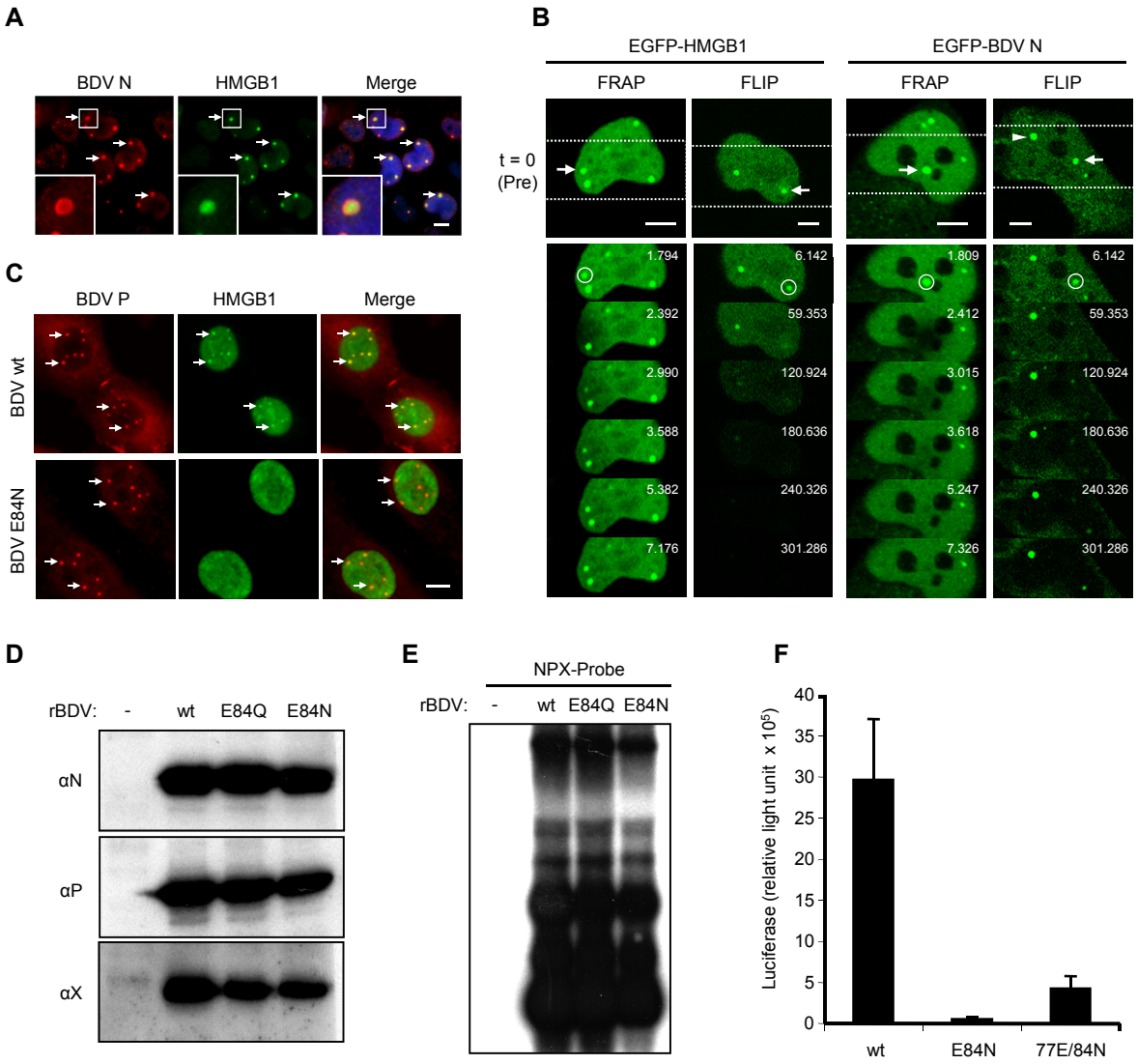

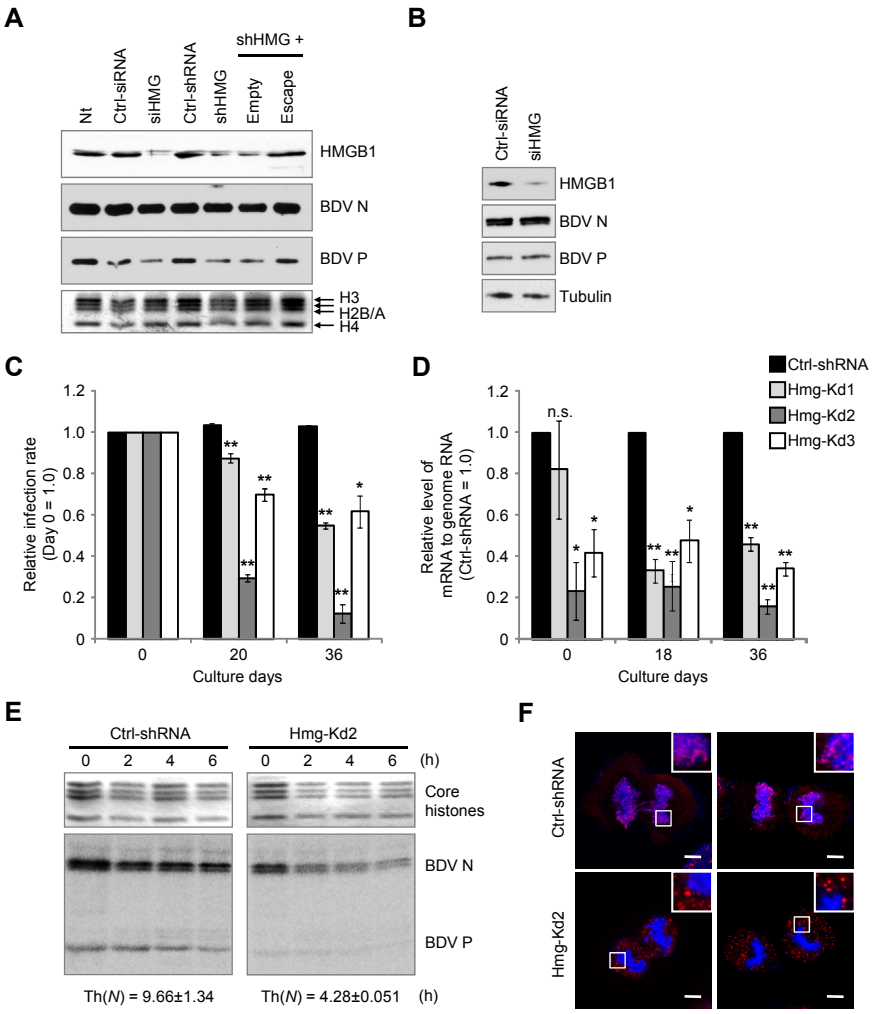

Cell Host & Microbe,

Supplemental Information

Intranuclear persistence of bornavirus reveals a new life cycle of RNA virus closely associated with host chromosome

Yusuke Matsumoto, Yohei Hayashi, Hiroko Omori, Tomoyuki Honda, Takuji Daito, Masayuki Horie, Kazuyoshi Ikuta, Kan Fujino, Shoko Nakamura, Urs Schneider, Geoffrey Chase, Tamotsu Yoshimori, Martin Schwemmle and Keizo Tomonaga

Inventory of Supplemental Information

1. Supplemental experimental procedures

2. Supplemental references

3. Supplemental figures

   Figure S1: related to Figure 2
   Figure S2: related to Figure 3
   Figure S3: related to Figure 4
   Figure S4: related to Figure 5
   Figure S5: related to Figure 6
   Figure S6: related to Figure 7

SUPPLEMENTAL EXPERIMENTAL PROCEDURES

Plasmids

The enhanced green fluorescent protein (EGFP)-fused eukaryotic expression vectors (pEGFP-N and pEGFP-HMGB1) used for FRAP and FLIP analyses were constructed as previously described (Kobayashi et al., 2001; Pallier et al., 2003; Yanai et al., 2006). The tandem tagged BDV N expression vector used for TAP analysis was generated as follows. BDV cDNA corresponding to the BDV N ORF was amplified using pcDL-N.wild as template. The PCR product was digested with *EcoR* I and *Xho* I and cloned into the vector for the TAP assay (kindly gift of Dr. Matsuura, Osaka University), to produce pTAP-N. The expression plasmid shRNA-resistant HMGB1 cDNA (HMGB1-Escape) was generated with no amino acid substitutions by introducing 16 nucleotide substitutions into two independent HMGB1 shRNA-target sites by PCR-based mutagenesis. Detailed information about the primers and PCR procedures used to generate these plasmids is available from the authors. The nucleotide sequences of the recombinant plasmids were confirmed by DNA sequence analysis.

Indirect immunofluorescence assays and microscopy

Cells were plated on Lab-Tek 2 chamber slides (Nalgene Nunc), fixed with 4% paraformaldehyde, and permeabilized for 5 min at room temperature with phosphate buffered saline (PBS) containing 0.4% Triton X-100. The cells were then incubated with antibodies (anti-BDV antibodies [Kobayashi et al., 2003; Watanabe et al., 2000], anti-HMGB1 antibody [BD Bioscience], anti-PARP1 polyclonal antibody [Active motif]) for 30 min in a humidified chamber at 37°C. This was followed by incubation with appropriate Alexa Fluor-conjugated secondary antibodies (Invitrogen). The cells were counterstained with 4’,6’-diamidino-2-phenylindole (DAPI) for 1 min at room temperature in PBS. For cell immunofluorescence imaging, an epifluorescence microscope E600 (Nikon Inc.) or a confocal laser-scanning microscope FV1000 (Olympus Inc.) was used for data collection.

FISH

Riboprobes for FISH were synthesized by using T7 RNA polymerase and DIG RNA labeling mix (Roche Diagnostics) according to the manufacturer's instructions. BDV-infected and -uninfected OL cells grown on slide glass (Matsunami glass Inc.) were fixed with 4% paraformaldehyde, and proteins were then denatured with 0.1 N HCl for 15 min. The cells

were then permeabilized with PBS containing 0.25% Triton X-100 for 5 min, washed with PBS, and endogenous peroxidase was inactivated with 0.5% H_5IO_6 in PBS for 10 min. For mitotic cells, the samples were treated with Proteinase K for 10 min at 37°C. After a wash with 2 × SSC (0.3 M NaCl-30 mM sodium citrate, pH 7.0), cells were incubated for 30 min at 37°C in hybridization buffer (50% formamide, 3 × SSC, 5 × Denhardt's solution [Nacalai Tesque Inc.], 250 µg/ml salmon sperm DNA [Invitrogen]), followed by a 15-h hybridization in hybridization buffer containing the denatured RNA probe at a concentration of 0.5 µg/ml at 37°C. The cells were then washed with 4 × SSC, 2 × SSC containing 2 µg/ml RNase A (Roche Diagnostics), and 0.2 × SSC. Fluorescence signal was detected by using anti-DIG-POD antibody (Roche Diagnostics) and TSA™-Plus Fluorescein System (PerkinElmer Inc.) according to the manufacturer's instructions.

TAP assay

A tandem affinity purification (TAP) assay was performed with chromatin-binding fractions derived from BDV-infected and uninfected OL cells transfected with pTAP-N. At 48 h post-transfection, a chromatin fraction was prepared and lysed with 0.1% Triton X-100 on ice for 30 min. After centrifugation, the soluble fraction was immunoprecipitated with anti-HA resin (Sigma-Aldrich) for 4 h at 4°C. The resin was washed three times with TNE buffer (10 mM Tris-HCl, pH 8.0, 150 mM NaCl, 1 mM EDTA, 0.1% Nonidet P-40 [NP-40], complete protease inhibitor) and the tagged protein was released from the resin by digestion with AcTEV protease (Invitrogen) in 150 µl of TEV buffer containing 10 U protease for 3 h at 16°C. TNE buffer was added to the supernatant from the centrifugation to increase the volume to 500 µl and the preparation was immunoprecipitated with anti-Flag M2 resin (Sigma-Aldrich) overnight at 4°C. After washing three times with TNE buffer, the resin was incubated with elution buffer (50mM Tris-HCl, pH 7.4, 150mM NaCl, complete protease inhibitor) containing 300 ng/µl of 3x Flag peptide (Sigma-Aldrich) for 90 min at 4°C. The eluates were analyzed by SDS-PAGE and visualized by silver staining (Wako). The protein bands of interest were excised, digested in-gel with trypsin, and analyzed by nanocapillary reversed-phase LC-MS/MS using a C18 column (φ 75 µm) on a nanoLC system (Ultimate, LC Packing) coupled to a quadrupole time-of-flight mass spectrometer (QTOF Ultima, Waters). Direct injection data-dependent acquisition was performed using one MS channel for every three MS/MS channels and dynamic exclusion for selected ions. Proteins were identified by database searching using Mascot Server (Matrix Science).

Immunoprecipitation

Chromatin-binding fractions prepared from BDV-infected OL cells were lysed with 0.1% Triton X-100 on ice for 30 min and clarified by centrifugation for 10 min at 15,000 rpm. MNase buffer containing 5 mM EDTA-EGTA and 0.1% Triton X-100 was added to the supernatants to increase the volumes to 500 µL and they were incubated overnight with Protein-A Sepharose CL-4B (GE Healthcare Science), pre-coated with polyclonal antibody against BDV N. After washing three times with TNE buffer, the immunoprecipitates were eluted with elution buffer (50 mM glycine, pH 2.5) and analyzed by SDS-PAGE. For immunoprecipitation of H2A, H2B, Orc2 and Mek2, the following antibodies were used: anti-H2A and -H2B polyclonal antibodies (Upstate, 07-146 and 07-371), anti-Orc2 polyclonal antibody (BD Bioscience, 559266), anti-Mek2 antibody (Cell Signaling, 9125).

Quantitative real-time RT-PCR

Chromatin-bound vRNA was extracted from the chromatin-binding fractions described above and reverse transcribed with a Transcriptor First Strand cDNA Synthesis Kit (Roche) using a BDV-specific primer (5'-TGT TGC GCT AAC AAC AAA CCA ATC AC-3') or an anchored oligo(dT) primer. Quantitative real-time RT-PCR assays were carried out using a gene-specific double fluorescent-labeled probe in the 7900HT Fast Real-Time PCR System (Applied Biosystems). The Taqman® probe was labeled with 6-carboxy fluorescein (FAM) as the 5' fluorescent reporter and tetramethylrhodamine (TAMRA) as the 3' quencher. The primers and probe used were as follows: BDV P-forward primer, 5'-ATG CAT TGA CCC AAC CAG TC-3'; BDV P-reverse primer, 5'-ATC ATT CGA TAG CTG CTC CCT TC-3'; and BDV P-probe, 5'-FAM-AGA ACC CCT CCA TGA TCT CAG ACC CAG A-TAMRA-3'. The amount of the first template was measured as follows. The threshold cycle (Ct) value was determined as the number of cycles at which a significant fluorescence increase was first detected. The threshold was automatically defined by the Sequence Detection System (ABI). The Ct-value was converted to signal intensity using a method that assumes the difference of 1 cycle between samples reflects a 2-fold difference. The relative amounts of BDV vRNA between euchromatin and heterochromatin were determined by the correlation with the amounts of core histones isolated from each chromatin fraction.

Pulse-chase analysis

shRNA-expressing or control BDV-infected cells grown on 60 mm diameter dishes were washed twice with pre-warmed PBS and starved for 1 h at 37°C in labeling medium (Met/Cys-free high glucose DMEM; Gibco). Cells were labeled with 150 μCi [^{35}S]methionine/cysteine/ml for 30 min at 37°C and chased for the indicated times in growth medium. After the chase, cells were subjected to chromatin-binding assays and then immunoprecipitated with anti-BDV N polyclonal antibody as described above. To calculate the half-life of chromatin-bound BDV N protein, Th(*N*), pulse-labeled BDV N was detected by Bass 2000 and normalized to the input histone H4 density visualized by Coomassie blue staining.

SUPPLEMENTAL REFERENCES

Kobayashi, T., Kamitani, W., Zhang, G., Watanabe, M., Tomonaga, K., and Ikuta, K. (2001). Borna disease virus nucleoprotein requires both nuclear localization and export activities for viral nucleocytoplasmic shuttling. J. Virol. *75*, 3404-3412.

Kobayashi, T., Zhang, G., Lee, B.J., Baba, S., Yamashita, M., Kamitani, W., Yanai, H., Tomonaga, K., and Ikuta, K. (2003). Modulation of Borna disease virus phosphoprotein nuclear localization by the viral protein X encoded in the overlapping open reading frame. J. Virol. *77*, 8099-8107.

Pallier, C., Scaffidi, P., Chopineau-Proust, S., Agresti, A., Nordmann, P., Bianchi, M.E., and Marechal, V. (2003). Association of chromatin proteins high mobility group box (HMGB) 1 and HMGB2 with mitotic chromosomes. Mol. Biol. Cell *14*, 3414-3426.

Yanai, H., Kobayashi, T., Hayashi, Y., Watanabe, Y., Ohtaki, N., Zhang, G., de la Torre, J.C., Ikuta, K., and Tomonaga, K. (2006). A methionine-rich domain mediates CRM1-dependent nuclear export activity of Borna disease virus phosphoprotein. J. Virol. *80*, 1121-1129.

Watanabe, M., Zhong, Q., Kobayashi, T., Kamitani, W., Tomonaga, K., and Ikuta, K. (2000). Molecular ratio between borna disease viral-p40 and -p24 proteins in infected cells determined by quantitative antigen capture ELISA. Microbiol. Immunol. *44*, 765-772.

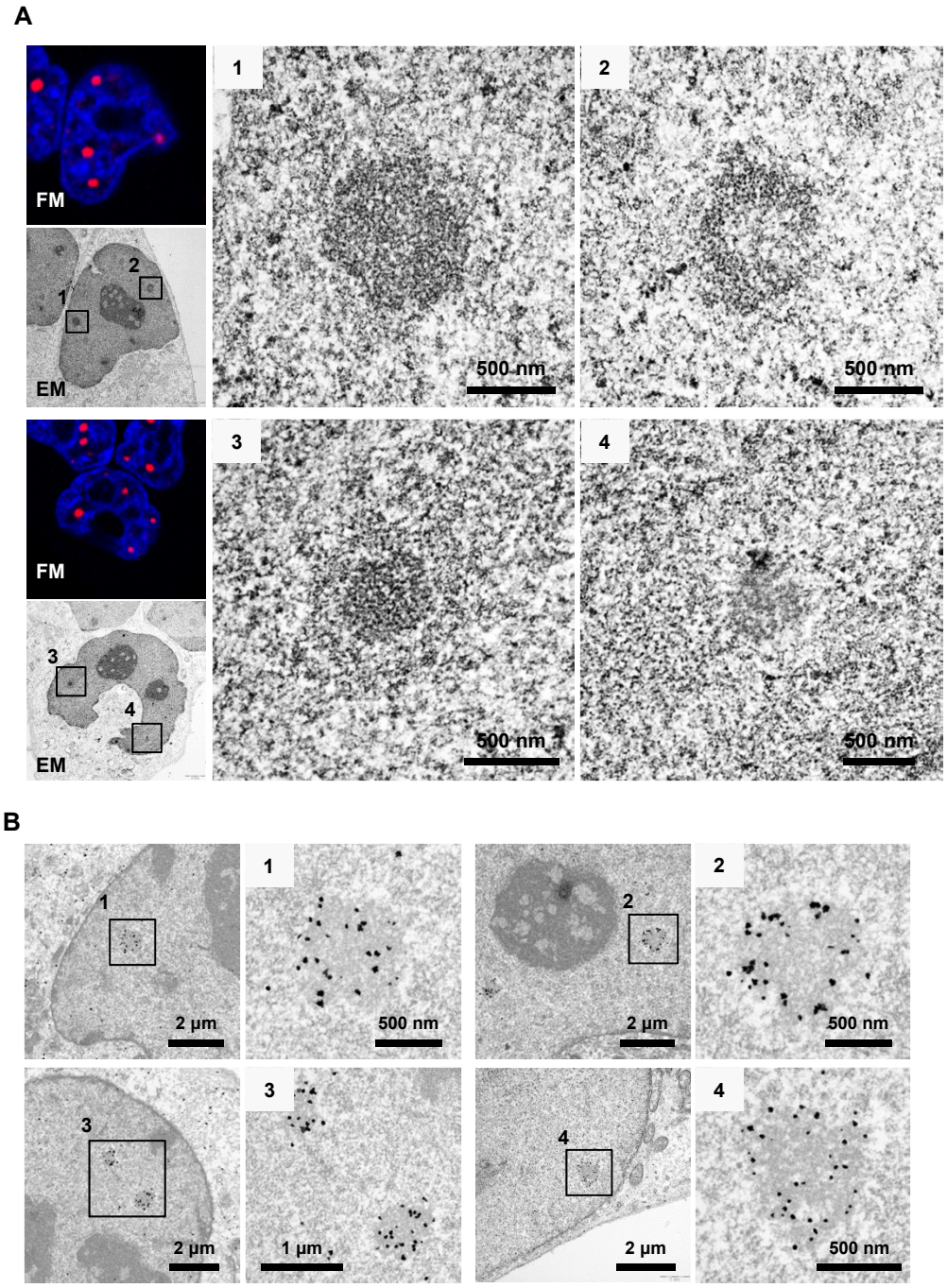

Figure S1. Correlative FM-EM and immuno-EM analyses of interphase, BDV-infected cells. (related to Figure 2)

(**A**) BDV-infected OL cells stained by anti-N antibody (red) and DAPI (blue) were analyzed by immunofluorescence microscopy and the same fields were analyzed under EM. (**B**) Immuno-EM images of vSPOT in BDV-infected stained with anti-BDV N antibody. A magnification of boxed area is shown in the right panel. Scale bars are indicated.

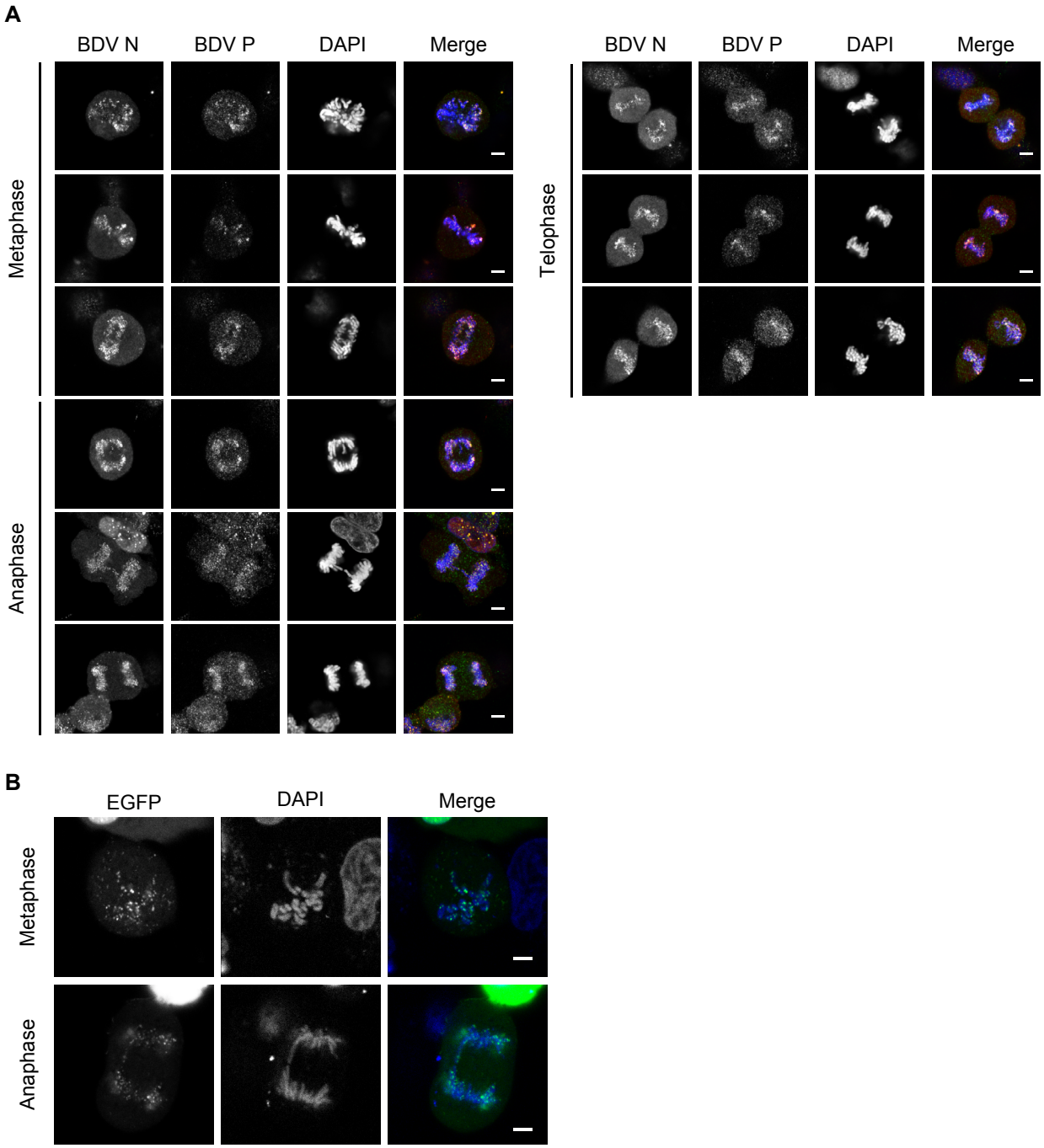

Figure S2. Association of BDV RNP with mitotic chromosomes. (related to Figure 3)

(**A**) The mitotic stages (metaphase, anaphase and telophase) of BDV-infected OL cells were stained by anti-BDV N (red) and anti-BDV P (green) and DAPI (blue) and analyzed by confocal microscopy. Scale bar, 5 μm. (**B**) The EGFP-fused BDV N expression plasmid was transfected into OL cells infected with BDV, and the EGFP signal was monitored by fluorescence microscopy. The metaphase and anaphase nuclei were visualized by DAPI staining. Scale bar, 5 μm.

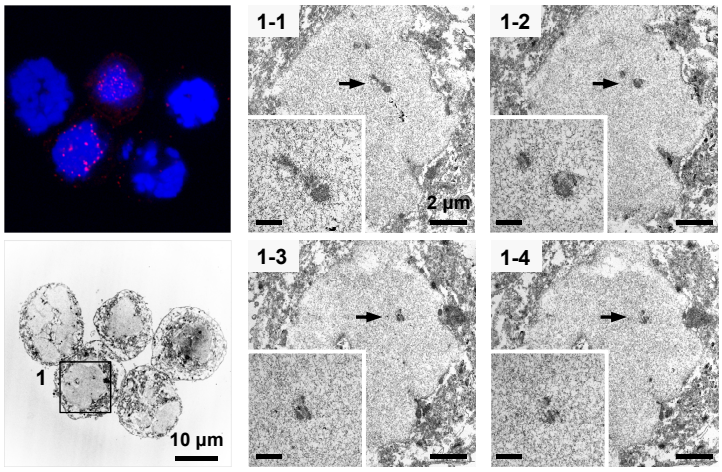

Figure S3. Serial section correlative FM-EM analyses of metaphase chromosomes of BDV-infected cells. (related to Figure 4)

Metaphase chromosomes of BDV-infected cells were stained by anti-N antibody (red) and DAPI (blue) and examined by immunofluorescence microscopy. The same fields were then analyzed by EM. Serial sections (90 nm) were generated for EM observation. Magnifications of the boxed and pointed area are shown. Scale bars in the insets, 500 nm.

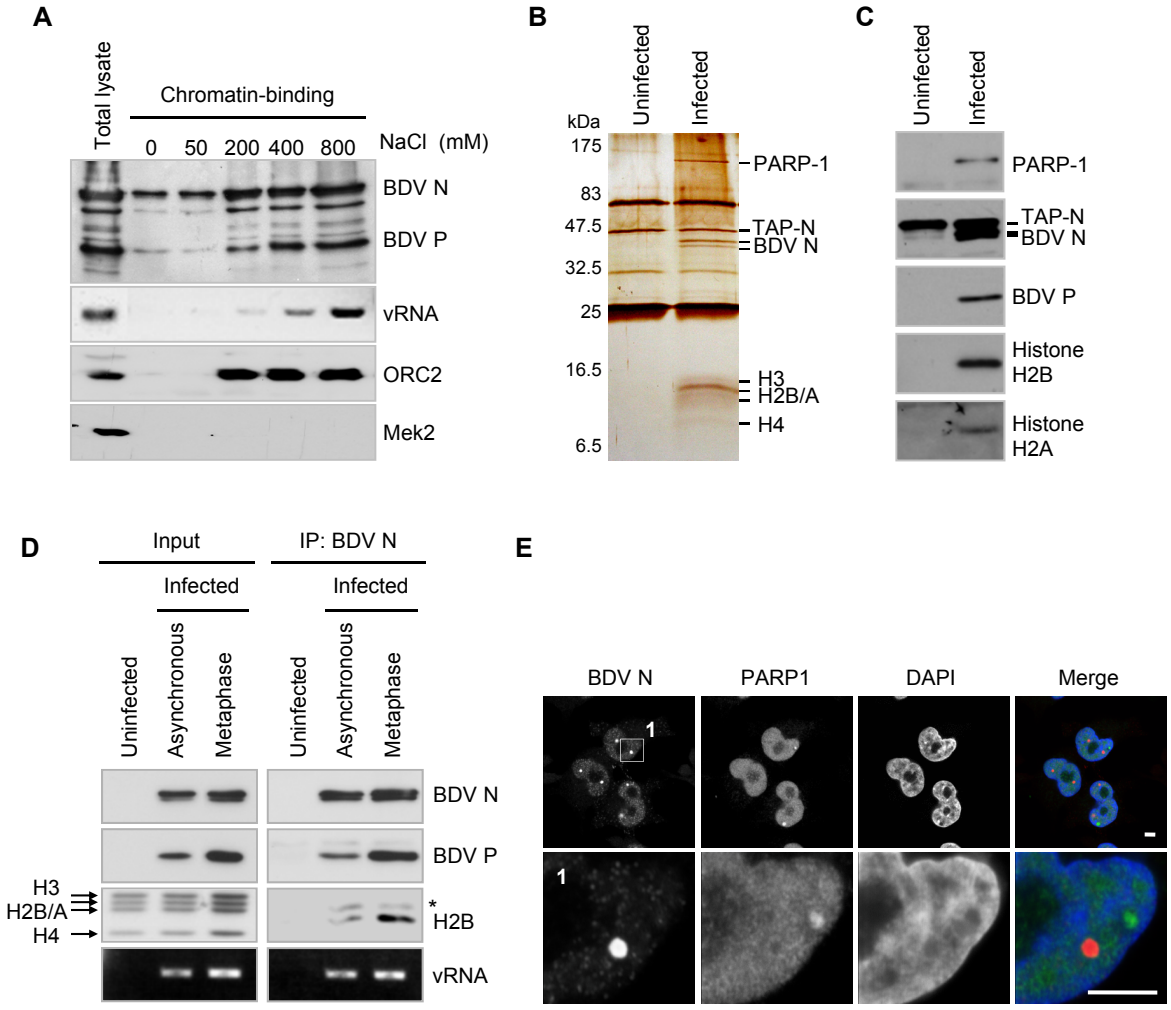

Figure S4. BDV RNP associates with chromatin via binding to core histones. (related to Figure 5)

(**A**) Salt extraction of BDV RNPs from the chromatin-binding fraction. The nuclei of BDV-infected OL cells were incubated with buffer A containing 0, 50, 200, 400, and 800 mM NaCl and extracted for 30 min at 4 ºC. The supernatants, containing proteins released from the nuclei, were recovered by centrifugation, and western blotting was performed with anti-BDV N and P polyclonal antibodies. BDV vRNA was detected by RT-PCR using specific primers for BDV genome RNA. ORC2 (chromatin-associated human protein) and Mek2 (cytosolic kinase) were used as fractionation controls. Total lysate: total cellular extract of BDV-infected OL cells. (**B** and **C**) Tandem-affinity purification analysis of BDV N. Proteins that co-precipitated with TAP-N in BDV-infected cells were separated by SDS-PAGE, visualized by silver staining (**B**), and identified by western blotting (**C**). (**D**) H2B and MNase-resistance vRNA were immunoprecipitated by anti-N antibody (IP) from the chromatin-binding fractions of asynchronous and metaphase-arrested BDV-infected OL cells. H2B was detected by western blotting. Asterisk indicates a non-specific band. Core histones in the input panel were visualized by Coomassie blue. (**E**) Distribution of PARP-1 in BDV persistently infected nucleus. BDV-infected OL cells were stained by anti-PARP-1 (green) and BDV N (red) antibodies. The nuclei were visualized by DAPI staining. PARP-1 appeared to not colocalize with vSPOT in the infected nuclei. Magnifications of the boxed area are shown. Scale bar, 5μm.

A

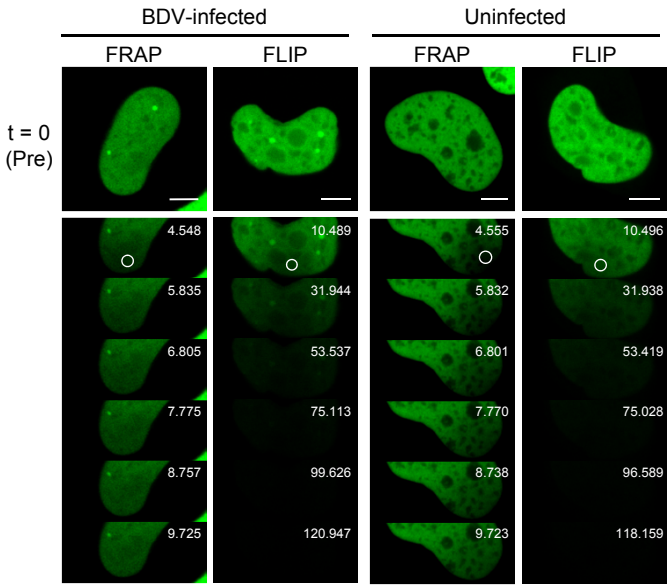

B

BDV P (aa 74-88)	P mutants	MTH HMGB1	MTH P	MTH N	MTH X	MR
L_{74}IKKLVTELAENSMI$_{88}$	P wt	+	+	+	+	++
L_{74}IKAAVTELAENSMI$_{88}$	P-K77AL78A	+	+	+	+	n.d
L_{74}IKKLAAELAENSMI$_{88}$	P-V79AT80A	+	+	+	+	+
L_{74}IKKLVTAAAENSMI$_{88}$	P-E81AL82A	-	+	+	-	-
L_{74}IKKLVTELAANSMI$_{88}$	P-E84A	-	+	+	+	-
L_{74}IKKLVTELAAAAMI$_{88}$	P-N85AS86A	+	+	+	+	n.d
L_{74}IKKLVTELANAAMI$_{88}$	P-E84N	-	+	+	+	++
L_{74}IKKLVTELAQAAMI$_{88}$	P-E84Q	-	+	+	+	++

C

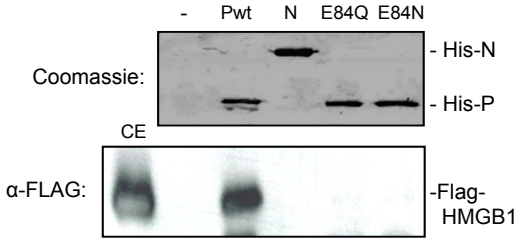

D

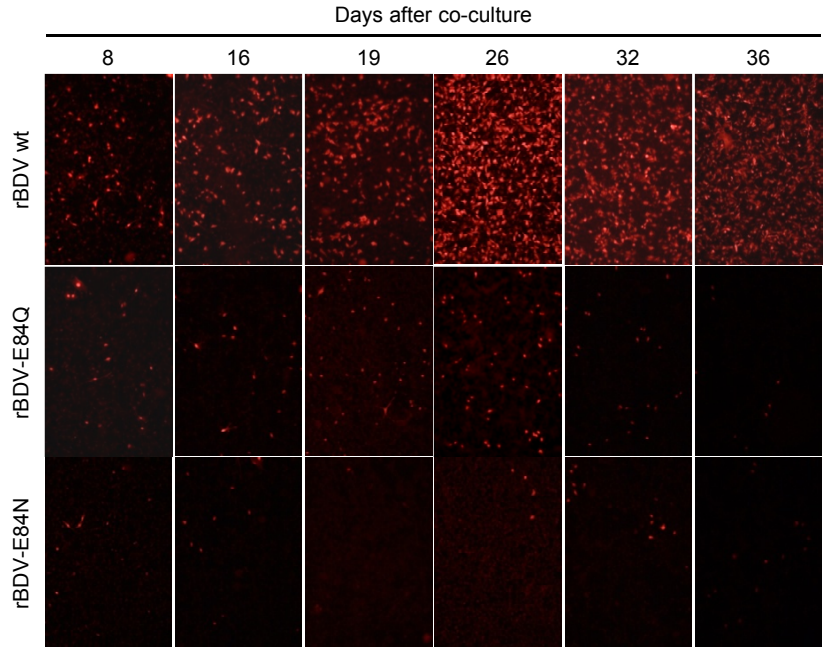

Figure S5. FRAP and FLIP analyses of EGFP-HMGB1 and generation of rBDVs that lack the interaction with HMGB1. (related to Figure 6)

(**A**) BDV-infected and uninfected OL cells expressing EGFP-HMGB1 were imaged before (t = 0) and during FRAP or FLIP of a chromatin area in the nucleus. Images were taken at the times (s) indicated. The bleached spots are indicated by white circles. Scale bar, 5 μm. (**B**) BDV P mutants with the indicated amino acid substitution in the HMGB1 binding region were tested for efficient protein-protein interaction with viral nucleocapsid protein (nucleoprotein [N], X protein [X] and wt P [P]) and rat HMGB1 in the mammalian-two hybrid (MTH) system and for their activity in the BDV minireplicon assay (MR). (+) unimpaired activity compared to wt P, (-) less than 3% activity compared to wt P. (**C**) The efficiency of BDV P mutants to bind rat HMGB1 in vitro were analyzed in an pull-down assay using *E. coli* purified histidine-tagged P mutants and N bound to Ni-agarose beads (upper panel). Bound material was analyzed by immunoblotting (IB) using anti-Flag antibodies. Note that in contrast to N, residual HMGB1 remains bound to the P mutants. CE, cell extract. **(D)** The rBDVs rescued by reverse genetics system in Vero cells were cocultured with puromycin-resistant OL cells, and three days after the co-culture, the selection with puromycin was added to the culture. The propagation of rBDVs (wild-type, E84N, and E84Q) were monitored by immunofluorescence assay using anti-N antibody at the indicated days after the co-culture.

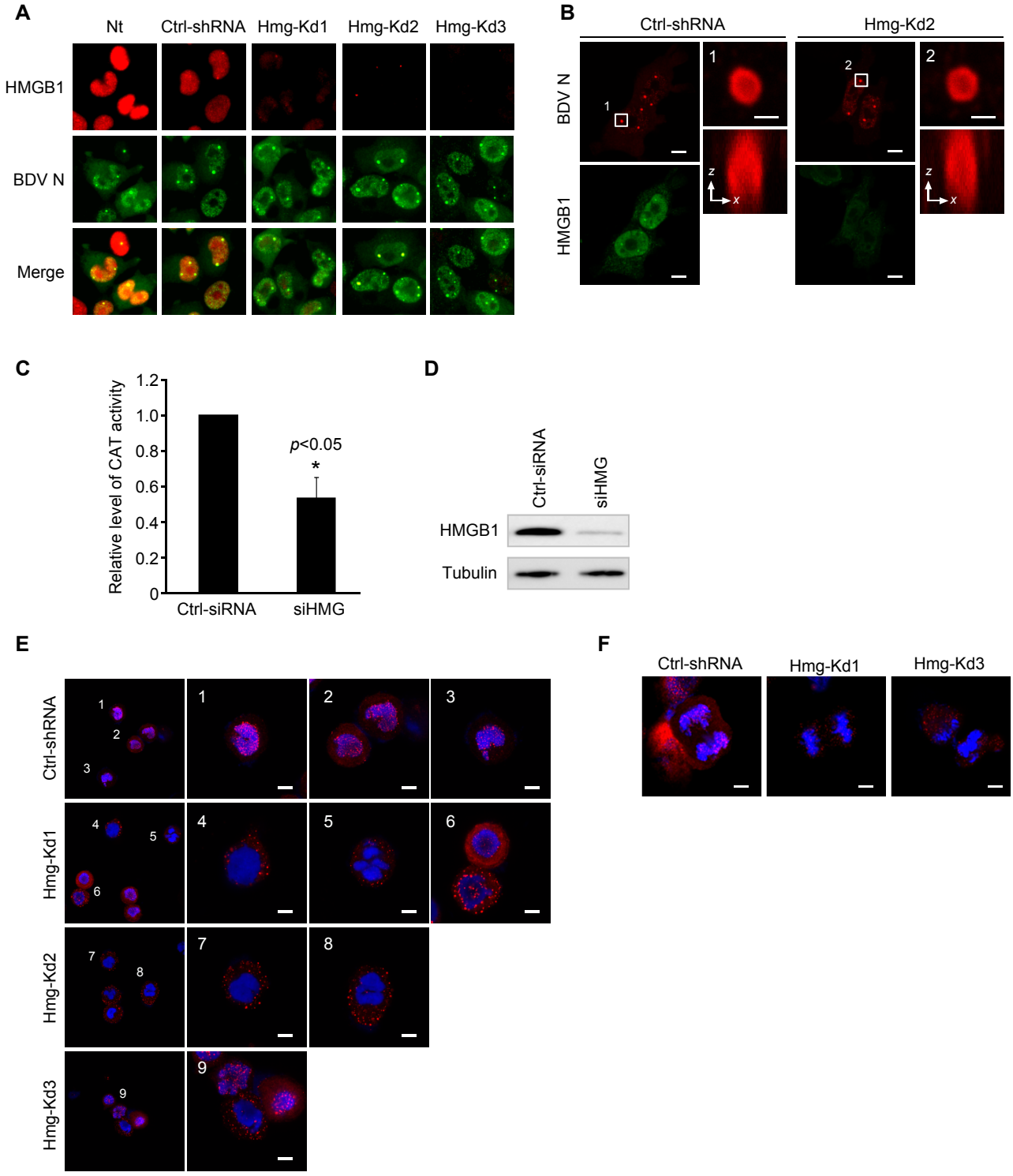

Figure S6. BDV dynamics in the nucleus of HMGB1-knockdown cells. (related to Figure 7)

(**A**) BDV-infected OL cells were infected with lentiviral vectors that encode shRNAs for HMGB1, and shRNA expression cells were selected by puromycin resistance. Two independent shRNAs were used for the knockdown. IFA for three different cell lines (Hmg-Kd1, -Kd2, and -Kd3) are shown. The cell lines were strained with anti-HMGB1 (red) and anti-BDV N (green) antibodies. Nt denotes non-treated BDV-infected cells. Ctrl-shRNA denotes cells treated with scrambled control shRNA. Hmg-Kd1 showed a mild knockdown of HMGB1 (< 70% based on the fluorescence intensity), whereas Hmg-Kd2 and -Kd3 showed a significant reduction of HMGB1 (< 90%). (**B**) Structure of vSPOT in HMGB1-kockdown, BDV-infected cells. Immunofluorescence analysis of HMGB1-knockdown (Hmg-Kd2) and Ctrl-shRNA-treated OL cells were performed with anti-BDV N (red) and HMGB1 (green) antibodies. Scale bar, 5 μm. Magnifications and detailed 3D structures of the boxed vSPOTs are shown on the right (Scale bar, 1 μm). A maximum z projection of 33 vertical slices (x-z plane) is shown. (**C** and **D**) BDV minireplicon assay using 293T cells treated with siRNA for HMGB1. Twenty-four hour after the transfection of siRNAs, 293T cells were transfected with BDV minireplicon plasmids, and 48 h later CAT activity in cell lysates was determined with the CAT-ELISA system (**C**). Relative CAT level from three independent experiments are expressed as mean plus SD. $*p < 0.05$. The expression of HMGB1 in the cells treated with ctrl-siRNA and siHMGB1 were detected by western blotting at 48 h posttransfection of minireplicon constructs. (**E** and **F**) Dissociation of BDV RNP from mitotic chromosomes in HMGB1-knockdown, BDV-infected cells. Immunofluorescence analysis of metaphase (**E**) and anaphase (**F**) of HMGB1-knockdown, BDV-infected (Hmg-Kd1, -Kd2, and -Kd3) and Ctrl-shRNA-treated, BDV-infected OL cell nuclei. The cells were stained with anti-BDV N antibody (red). The nuclei were visualized by DAPI staining. Magnifications and the numbered cells are shown on the right. HMGB1-knockdown appeared to abrogate the association of BDV RNPs with mitotic chromosomes. Scale bar, 5 μm.